J. Coord. Chem., 1994, Vol 32, pp. 173–212
Reprints available directly from the publisher
Photocopying permitted by license only

BIS(PORPHYRIN)ACTINIDE COMPLEXES AND THEIR RADICAL CATIONS AND DICATIONS

GREGORY S. GIROLAMI,* PHILIP A. GORLIN, STANLEY N. MILAM, KENNETH S. SUSLICK* and SCOTT R. WILSON

School of Chemical Sciences The University of Illinois at Urbana-Champaign 505 South Mathews Avenue Urbana, Illinois 61801

(Received October 5, 1993; in final form December 10, 1993)

The first bis(porphyrin)actinide complexes have been prepared by reaction of the diethylamide complexes $M(NR_2)_4$ (where M = Th, U and R = Me, Et) with 5, 10, 15, 20-tetraphenylporphyrin (H_2TPP) or 2, 3, 7, 8, 12, 13, 17, 18-octaethylporphyrin (H_2OEP). The coordination geometry of $Th(TPP)_2$ is a distorted square-antiprism where the thorium center is displaced 1.47 Å from each of the porphyrin N_4 planes; the porphyrin N_4 planes are threrefore separated by 2.94 Å. In $Th(OEP)_2$, the two porphyrin N_4 planes are separated by 2.89 Å in a nearly perfect square-antiprismatic coordination geometry around the thorium center. The porphyrin macrocycles, held in such close proximity, interact electronically as shown by a blue-shift in the porphyrin Soret band and by unusually low oxidation potentials relative to related monoporphyrin species. Chemical oxidations of $M(TPP)_2$ and of Th(OEP)(TPP) yield porphyrin-based radical cation complexes $[M(porph)_2^+][SbCl_6^-]$ and dicationic complexes $[M(porph)_2^{2+}][SbCl_6^-]_2$. The solid-state structure of $[Th(TPP)_2^+][SbCl_6^-]$ is nearly identical to that of $Th(TPP)_2$, but the separation between the N_4 planes decreases to 2.89 Å. The EPR spectra of $[Th(TPP)_2^+]$ and $[Th(OEP)(TPP)^+]$ are characteristic of simple organic radicals, while $[U(TPP)_2^+]$ shows unusual signals at $g_{\|} = 3.175$ and $g_{\perp} = 1.353$. The magnetic susceptibility of the paramagnetic (S = 1/2) complex $[Th(TPP)_2^+][SbCl_6^-]$ suggests that above 70 K there are thermally populated excited state(s) with f-orbital character. The uranium cation $[U(TPP)_2^+]$ apparently adopts an S = 1/2 ground state, in which the porphyrin radical is antiferromagnetically coupled to the f^2 U^{IV} center; at higher temperatures, the magnetic moment increases due to thermal population of S = 3/2 states. The thorium dicationic complexes are essentially diamagnetic. These results support the suggestion that direct porphyrin-porphyrin interactions yield new molecular orbitals that are composed of atomic orbitals from *both* porphyrin ligands; some contribution from metal f-orbitals is also possible. All of the oxidized complexes have near-IR absorptions due to transitions between these "supermolecular" orbitals. Crystal data for $Th(TPP)_2 \cdot C_7H_8$ at −25°C: orthorhombic, space group Fddd with $a = 21.635(5)$ Å, $b = 21.859(5)$ Å, $c = 31.119(6)$ Å, $\beta = 90.59(2)°$, $V = 14716(5)$ Å^3, $Z = 8$, $R_F = 0.054$, and $R_{wF} = 0.069$ for 333 variables and 3646 data with $I > 2.58\ \sigma(I)$. Crystal data for $Th(OEP)_2$ at 28°C: monoclinic, space group $P2_1/n$ with $a = 15.699(1)$ Å, $b = 15.474(1)$ Å, $c = 26.318(2)$ Å, $\beta = 91.97(1)°$, $V = 6389(2)$ Å^3, $Z = 4$, $R_F = 0.031$, and $R_{wF} = 0.038$ for 734 variables and 6059 data with $I > 2.58\ \sigma(I)$. Crystal data for $[Th(TPP)_2^+][SbCl_6^-] \cdot 2C_7H_8 \cdot CH_2Cl_2$ at 26°C: tetragonal, space group P_4/nnc with $a = 19.104(3)$ Å, $b = 19.104(3)$ Å, $c = 26.335(3)$ Å, $V = 9612(5)$ Å^3, $Z = 4$, $R_F = 0.065$, and $R_{wF} = 0.106$ for 248 variables and 1894 data with $I > 2.58\ \sigma(I)$.

KEYWORDS: actinide, metalloporphyrin, porphyrin, sandwich complexes, Special Pair

INTRODUCTION

Metalloporphyrin complexes that contain two porphyrin ligands per metal center have been reported for yttrium,[1] most of the lanthanides,[2] Th and U,[3] and recently

* Authors for correspondence.

for Zr and Hf.[4] Complexes of this type are of fundamental interest as structural models of the photosynthetic reaction center, which in bacteria such as *Rhodopseudomonas viridis* have two bacteriochlorophyll units arranged in a face-to-face manner ≈3 Å apart.[5] This ≈3 Å separation is also characteristic of bis(porphyrin)-metal complexes. Apart from their utility as structural models, bis(porphyrin)metal complexes also possess spectroscopic and chemical properties similar to the special pair.[6] In particular, the photochemical and electrochemical behavior of these complexes may provide key insights into the photoredox process (photon in, electron out), which is the primary function of the special pair. In addition, it is possible to modify the bis(porphyrin)metal complexes chemically and observe how such chemical modifications affect the photochemical and electrochemical behaviour.[7] Such an approach is difficult to apply to the naturally occurring photosynthetic system, since at present it is not possible to carry out specific chemical modifications of the natural system in a controlled fashion.

The sandwich complexes with a tetravalent metal (Th, U, Ce, Zr, and Hf) contain two "normal" (*i.e.* non-radical) porphyrin ligands. In contrast, the trivalent landthanide complexes contain one porphyrin(1-) radical ring and one "normal" porphyrin(2-) ring. Such an electronic configuration can be achieved for the $M^{IV}(porph)_2$ compounds by chemical or electrochemical oxidation. The π-radical cations formed exhibit an intense broad band in the near-IR region (at *ca.* 1000-1400 nm) that is similar to a band observed for the oxidized photosynthetic site of *R. viridis*.[6a] Interestingly, the energy of the NIR band is related to the interporphyrin separation, which in turn depends on the size of the central metal. Larger metals increase the interplanar distance and lower the energy of the NIR transition. Resonance Raman and electronic studies suggest that the unpaired electron in the cationic $M^{IV}(porph)_2^+$ and the neutral $M^{III}(porph)_2$ complexes is delocalized over both porphyrin macrocycles on both the electronic and vibrational time scales.[8] Bocian has proposed that the HOMO π orbitals of the porphyrin monomers overlap strongly because they are held in close proximity. The strong overlap results in new "supermolecular" bonding and antibonding molecular orbitals which contain contributions from both porphyrin ligands and perhaps the metal center as well. The NIR absorption is thus proposed to arise from an electronic transition between the porphyrin-porphyrin bonding and antibonding orbitals. This model has been convincingly supported by detailed investigations of the photophysical properties of both the ground state and electronic excited states of several sandwich complexes.[9]

We now wish to describe full details of the synthesis and characterization of the first bis(porphyrin)actinide complexes. The X-ray crystal structures of $Th(TPP)_2$, $Th(OEP)_2$, and $[Th(TPP)_2^+][SbCl_6^-]$ are also reported. Some of this work has been reported in preliminary form.[3]

RESULTS

Preparation of the Bis(porphyrin) Complexes

Treatment of the tetrakis(diethylamide) or tetrakis(dimethylamide) complexes $Th(NR_2)_4$ or $U(NR_2)_4$ with two equivalents of tetraphenylporphyrin, H_2TPP, in refluxing toluene gives a purple insoluble product in each case. The insoluble

product is washed exhaustively with toluene to remove unreacted H_2TPP and then is chromatographed on silica gel with chloroform as the eluent. The $M(TPP)_2$ complexes (M = Th, M = U) move with the solvent front as a broad band and are thus separated from a small slow-moving impurity band. The resultant chloroform solution is filtered and taken to dryness to give the analytically pure product.

The analogous bis(octaethylporphyrin) sandwich complexes, $Th(OEP)_2$ and $U(OEP)_2$, can be made by treatment of the corresponding $M(NEt_2)_4$ complex with two equivalents of octaethylporphyrin, H_2OEP, in refluxing toluene. The product is separated from unreacted H_2OEP by removing the toluene and extracting the residue with pentane, in which the $M(OEP)_2$ products are quite soluble. Other contaminants can be removed by applying the pentane extract to a short column of silica gel and washing exhaustively with pentane. The $M(OEP)_2$ complexes do not move on silica gel with pentane as the eluent. The silica gel at the top of the column can then be removed and extracted with chloroform; taking the chloroform extract to dryness yields the deep purple $M(OEP)_2$ sandwich compounds. Trace amounts of H_2OEP, if present, may be removed by treatment with excess p-toluenesulfonic acid in chloroform followed by chromatography using chloroform as the eluent.

The mixed sandwich compound Th(OEP)(TPP) may be similarly prepared by using one equivalent each of H_2TPP and H_2OEP. Separation of the desired mixed porphyrin product from $Th(TPP)_2$ and $Th(OEP)_2$ and also from unreacted freebase porphyrins can be accomplished by chromatography on silica gel. Using toluene/hexane as the eluent, the unreacted free base porphyrins elute first, followed by Th(OEP)(TPP). If desired, the $Th(TPP)_2$ formed can then be eluted with methylene chloride. No $Th(OEP)_2$ was eluted, probably because it is oxidized to the π-radical cation on the column. We and others have observed similar oxidation of $Zr(OEP)_2$ on silica gel.[4a,c]

Spectroscopic Characterization of the M(porph)$_2$ Complexes

Porphyrins and their complexes with transition metals are commonly characterized by the location of the intense Soret band near 400 nm and the several less intense Q-bands between 400 and 700 nm.[10] In general, metallation of a porphyrin results in a red-shift of the Soret band and collapse of the several Q-bands to one or two bands. The Soret bands of the bis(TPP) actinide complexes are located at 402 nm for $Th(TPP)_2$ and 404 nm for $U(TPP)_2$ (Figure 1); in both cases the Soret bands are higher in energy than the 418 nm Soret band in H_2TPP. This blue-shifting of the Soret band, therefore, contrasts with the behavior of most 1:1 metal:porphyrin complexes. Both complexes have several Q bands, the most prominent appearing at 553 nm and 550 nm, respectively. In addition, new Q bands appear near 480 and 615 nm which are not seen in monomeric metalloporphyrins and thus must arise from the substantial π-π interactions present in bis(porphyrin) complexes. A discussion of the electronic origin of these bands has been presented elsewhere,[9] and will be briefly outlined in the Discussion Section.

As was observed for the TPP analogs, the Soret bands of $Th(OEP)_2$, 381 nm, and $U(OEP)_2$, 386 nm, are blue-shifted relative to that of H_2OEP (400 nm). The Q bands in the thorium complex are observed at 533, 576, and 635 nm, while those in the uranium complex occur at 539, 583, and 663 nm. In support of the supermolecular MO model described earlier, the electronic spectrum of Th(OEP)-(TPP) is not a superposition of OEP and TPP spectra, which would imply that

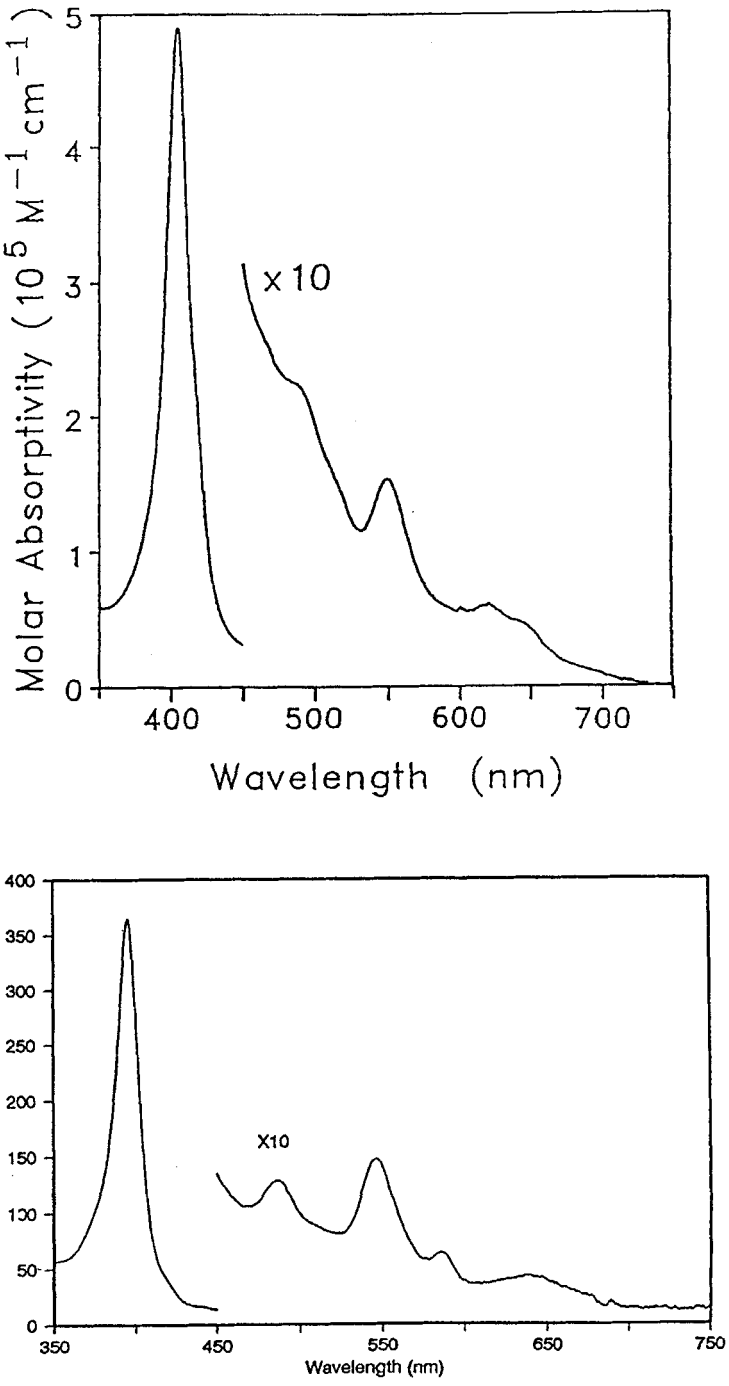

Figure 1 UV-Visible spectra of $Th(TPP)_2$ (top) and Th(OEP)(TPP) (bottom) in $CHCl_3$.

the two porphyrin rings are weakly interacting. Instead, a narrow Soret band is seen at 393 nm, with Q bands present at 486, 544, 584, and 638 nm (Figure 1).

The ^{1}H NMR spectrum of $Th(TPP)_2$ at $-20°C$ in $CDCl_3$ (Figure 2) reveals six well-resolved signals that may be assigned to the pyrrole hydrogens (δ 8.32) and five phenyl hydrogens (δ 9.33, 8.06, 7.73, 7.27, and 6.57), which have been assigned

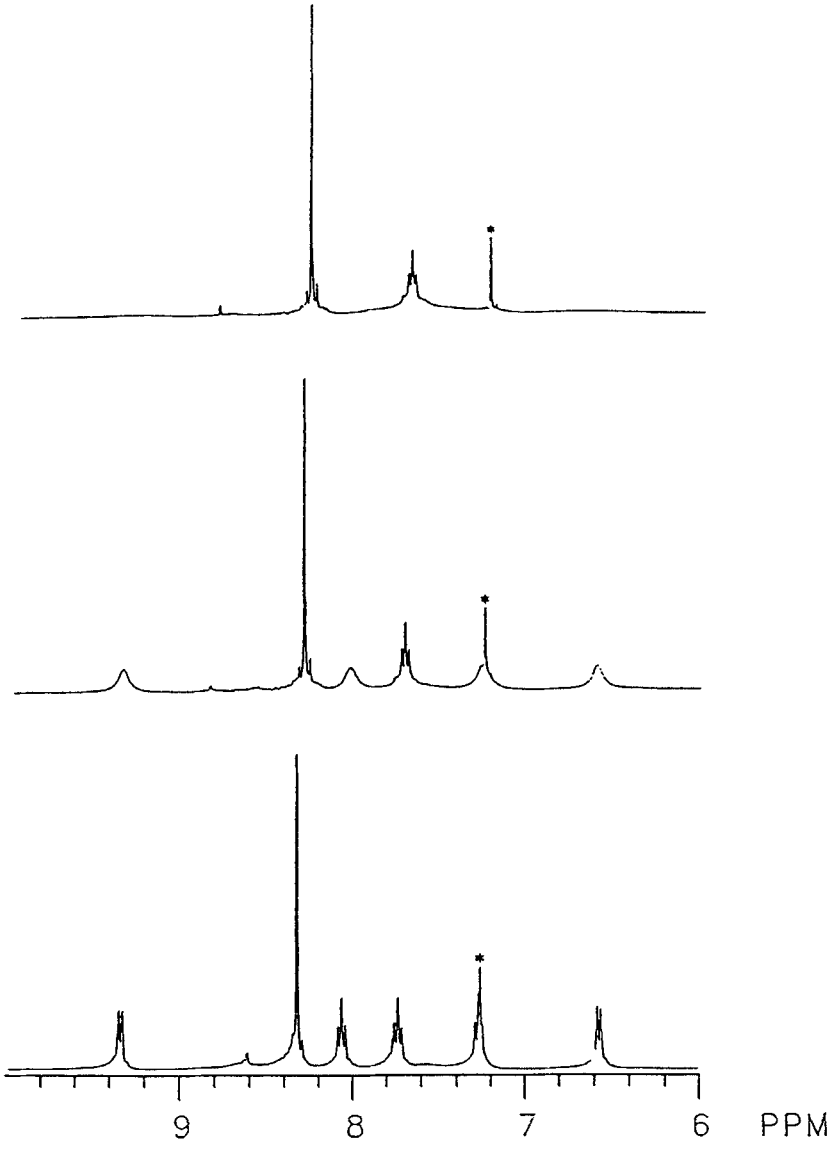

Figure 2 360 MHz ^{1}H NMR spectrum of $Th(TPP)_2$ in $CDCl_3$ at -20°C (bottom), + 20°C (middle), + 50°C (top). The residual $CHCl_3$ peak is marked with an asterisk.

based on the observed multiplicities and intensities (see Experimental Section). The pattern of phenyl proton signals from low field to high field (ortho, meta, para, meta, and ortho) is preserved in other actinide porphyrin complexes,[11] and may be used to aid assignment of signals where multiplicities are not observable. The presence of five signals for the phenyl protons is consistent with the fact that in the $M(TPP)_2$ molecules, the porphyrin macrocycles are not molecular mirror planes as they are in the free H_2TPP porphyrin molecule. Furthermore, rotation of the phenyl groups about the C–C bond that connects them to the porphyrin core must be slow on the NMR time scale at −20°C.

Although $Th(TPP)_2$ is diamagnetic, the linewidths of four of the signals are temperature dependent. The sharp ortho doublets and meta triplets seen at -20°C broaden and vanish at 50°C, while the para triplet and pyrrole singlet remain sharp (Figure 2). The temperature dependence of the proton NMR spectrum of $Th(TPP)_2$ is the result of rotation of the phenyl rings about their bonds to the porphyrin core. The slow exchange limit spectrum seen at −20°C changes at 50°C to an intermediate exchange spectrum near the coalescence temperature where the ortho and meta proton signals have broadened into the baseline. The para proton and pyrrole proton signals are not affected by the rotational process as they cannot undergo exchange. From the exchange parameters $T_c = 333$ K and $\Delta\nu = 998$ Hz, the rotation barrier for the phenyl groups in $Th(TPP)_2$ can be calculated to be $\Delta G^{\ddagger} = 14.5$ kcal/mol; this is comparable to the 13.8 kcal/mol value obtained for the same process in the thorium monoporphyrin complex $Th(TPP)Cl_2$.[11] The similarity of the activation energies of phenyl ring rotation in the mono- and bis(porphyrin) complexes suggests that the rotation is not unusually hindered in $Th(TPP)_2$, despite the close proximity of the two porphyrin rings.

The ^1H NMR spectrum of $U(TPP)_2$ in $CDCl_3$ at 20 °C is analogous to that of $Th(TPP)_2$ except that the paramagnetism of the f^2 uranium center broadens and shifts the resonances. The chemical shifts of the signals are temperature dependent and, the Curie plots of the chemical shifts δ *vs* T^{-1} are all linear (Figure 3). The phenyl proton signals extrapolate to the δ 6 to δ 9 region and the pyrrole proton signal extrapolates to δ 10.6 in the diamagnetic limit ($T^{-1} \rightarrow 0$). These extrapolated values are very similar to the chemical shifts of $Th(TPP)_2$.

The ^1H NMR spectrum of $Th(OEP)_2$ at room temperature in $CDCl_3$ has four signals at δ 9.18 (meso-H), 4.11 (CH_2), 3.89 (CH_2), and 1.70 (CH_3). This spectrum is quite similar to those reported for related $M(OEP)_2$ (M = Ce, Zr, Hf) analogs.[2b,4] The ^1H NMR spectrum of $U(OEP)_2$ at room temperature in $CDCl_3$ also has four signals at δ −1.17 (CH_3), −1.55 (CH_2), −3.43 (CH_2), and −5.25 (meso-H), but the chemical shifts are affected by the f^2 uranium center. The methylene protons of these complexes are diastereotopic and give rise to two doublets of quartets of equal intensity (AB part of an ABX_3 pattern). The diastereotopic nature of the methylene protons again confirms that the porphyrin ring planes are not molecular symmetry planes.

The ^1H NMR spectrum of Th(TPP)(OEP) in CD_2Cl_2 at room temperature exhibits signals for the two porphyrin rings (Figure 4). Thus, signals are observed at δ 9.47 (TPP o-H), 9.22 (OEP meso-H), 8.24 (TPP pyrrole), 8.22 (TPP m-H), 7.77 (TPP p-H), 7.31 (TPP m-H), 6.67 (TPP o-H), 4.14 (OEP CH_2), 3.86 (OEP CH_2), and 1.46 (OEP CH_3). One of the m-H signals is obscured by the β-pyrrole peak, but its presence can be shown by integration. The methyl OEP signal is shifted upfield

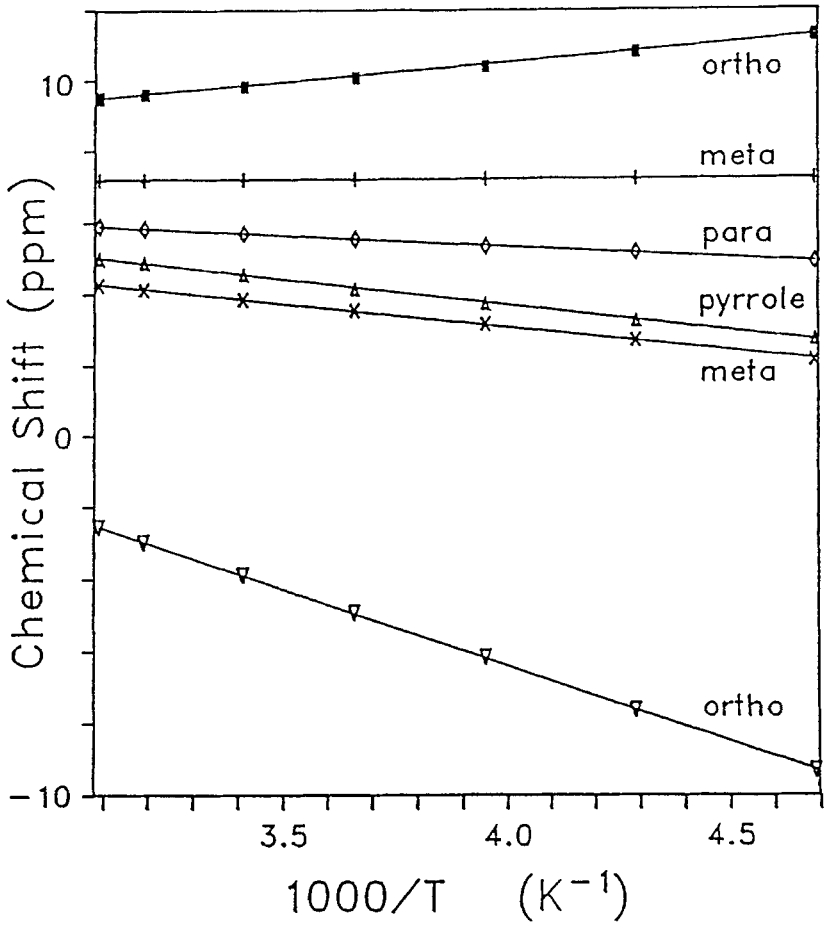

Figure 3 Curie plot of chemical shifts of $U(TPP)_2$ in $CDCl_3$ *vs.* T^{-1}.

from that in $Th(OEP)_2$, probably due to increased shielding due to the TPP ligand,[12] but otherwise the chemical shifts of both porphyrin rings are very similar to those observed in $Th(TPP)_2$ and $Th(OEP)_2$: the phenyl hydrogens of the TPP unit appear as five signals of equal intensity and the methylene protons of the OEP unit appear as an AB quartet.

Cyclic Voltammetry Studies

Cyclic voltammetry (CV) studies of 1 mM solutions of the $M(porph)_2$ complexes in CH_2Cl_2 reveal that the complexes undergo two chemically reversible oxidation processes (Table 1). The cathodic current equals the anodic current in both processes. For $Th(TPP)_2$, the redox waves are at 741 and 1089 mV *vs* Ag/AgCl, while for $U(TPP)_2$ they are at 625 and 1060 mV. The redox processes of the thorium complex must be porphyrin-based since the metal center is not oxidizable;

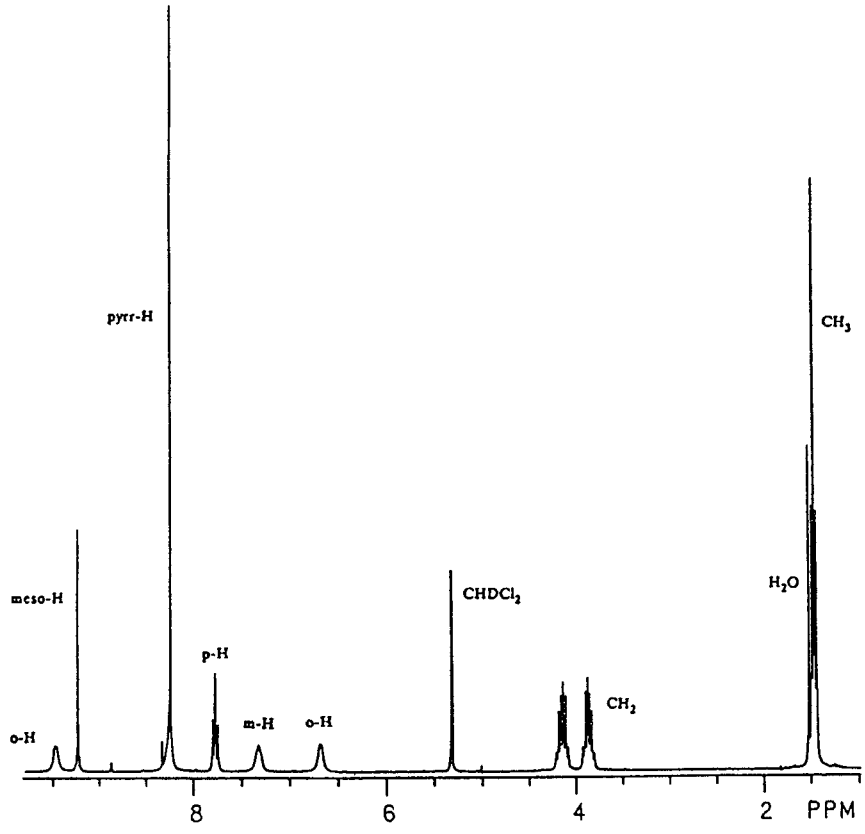

Figure 4 300 MHz ^{1}H NMR spectrum of Th(OEP)(TPP) in CD_2Cl_2 at 25°C.

the product of the first oxidation is therefore the radical cation $[Th(TPP)_2^+]$, while the product of the second oxidation must be the dication $[Th(TPP)_2^{2+}]$. The redox behavior of $U(TPP)_2$ is of particular interest since, at least in principle, the uranium(IV) center can itself be oxidized and reduced. However, the similarity of the voltammograms of $Th(TPP)_2$ and $U(TPP)_2$ suggest that the oxidation processes in the uranium complex are also largely porphyrin based. Nevertheless, the redox

Table 1 Oxidation potentials of the bis(porphyrin)actinide complexes.

Complex	Oxidation waves		Reduction waves	
$U(TPP)_2$	1060	625	-1415	-1721
$Th(TPP)_2$	1089	741	-1323	-1603
Th(OEP)(TPP)	1021	506	-1450	-1775
$Th(OEP)_2$	803	264	-1595	
$U(OEP)_2$	729	149	-1667	

All potentials measured in mV in CH_2Cl_2 *vs.* Ag/AgCl. [porph] = 1 mM; [^{n}Bu$_4$NPF$_6$] = 0.1 M. $FeCp_2$ oxidation under these conditions occurs at 510 mV.

potentials of $Th(TPP)_2$ and $U(TPP)_2$ are not identical: while the second oxidation is essentially unaffected by the nature of the metal, the first oxidation potentials differ by 116 mV. This difference is probably due to the smaller size of U^{4+} relative to Th^{4+}, although mixing of f-orbital character into the HOMO, especially in the uranium complex, cannot be ruled out.

The reduction processes for the $M(TPP)_2$ complexes also appear to be porphyrin-based. $Th(TPP)_2$ shows two one-electron reductions at −1323 and −1603 mV, while $U(TPP)_2$ undergoes similar reductions at −1415 and −1721 mV *vs.* Ag/AgCl. Again, the *ca.* 100 mV difference in redox potentials is probably ascribable to the smaller interplanar separation of the porphyrin rings in the uranium complex due to the smaller radius of uranium relative to thorium.

Cyclic voltammograms of $Th(OEP)_2$ and $U(OEP)_2$ are illustrated in Figure 5. Two oxidations and one reduction are observed for each complex. The reversible reductions occur at −1595 and −1667 mV for the thorium and uranium complexes, respectively. The similarities of the two reduction potentials strongly suggest that the two reduction processes are porphyrin-based and do not involve the metal. The two oxidation waves appear at 264 and 803 mV for $Th(OEP)_2$ and 149 and 729 mV for $U(OEP)_2$. Again, these are basically porphyrin-based processes.

In support of the view that there are strong π-π interactions in the bis(porphyrin) complexes, the redox potentials of Th(OEP)(TPP) are between those of $Th(OEP)_2$

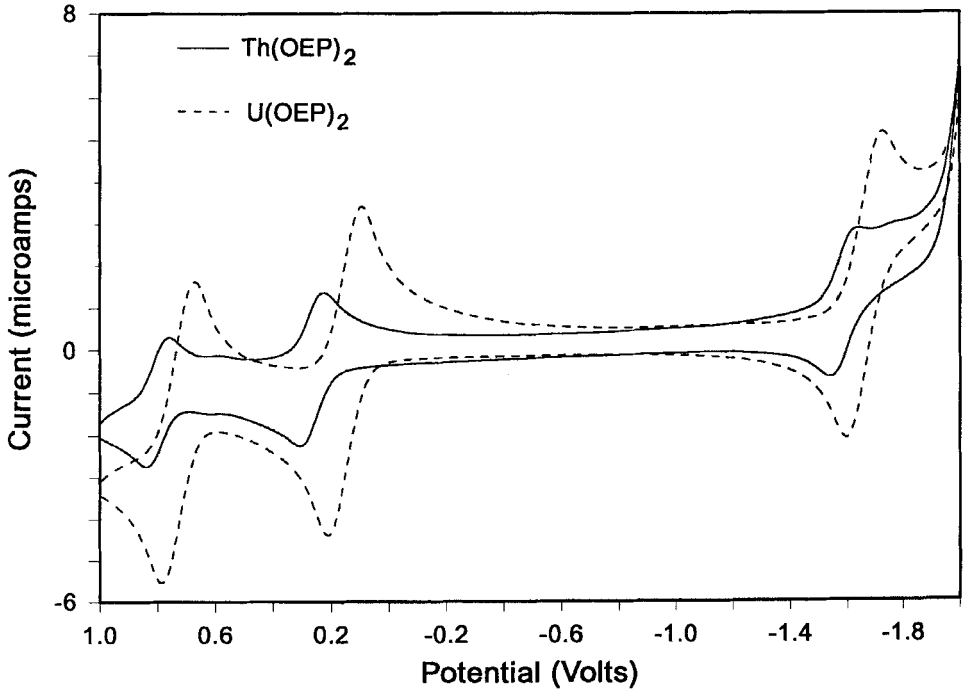

Figure 5 Cyclic voltammograms of $Th(OEP)_2$ (solid line) and $U(OEP)_2$ (dotted line) in CH_2Cl_2. Potentials are relative to Ag/AgCl. The porphyrin concentrations are *ca.* 1 mM. The concentration of $[^nBu_4N][PF_6]$ was 100 mM. Scan speed = 100 mV/sec.

and $Th(TPP)_2$ (Figure 6). Two oxidation waves are observed at 506 and 1021 mV *vs.* Ag/AgCl and two reductions are seen −1450 and −1775 mV. While the first oxidation is almost exactly the average of those of $Th(OEP)_2$ and $Th(TPP)_2$, the second oxidation of Th(OEP)(TPP) is much closer in potential to that of $Th(TPP)_2$.

Crystal Structures of $Th(TPP)_2 \cdot C_7H_8$ and $Th(OEP)_2$

In order to characterize these sandwich complexes more fully, X-ray diffraction analyses of $Th(TPP)_2$ and $Th(OEP)_2$ have been carried out. Suitable crystals of $Th(TPP)_2$ were grown in air by layering a chloroform solution of the porphyrin complex with toluene. After slow diffusion of the solvents, large, dark purple crystals formed. The complex crystallizes in the Fddd space group with one toluene molecule of crystallization per $Th(TPP)_2$ unit. Crystallographic data are presented in Table 2, atomic coordinates are given in Table 3, and selected bond distances and angles are collected in Table 4.

An ORTEP diagram of $Th(TPP)_2$ is illustrated in Figure 7. The diagram clearly reveals that the thorium atom is octacoordinate and adopts a distorted square antiprismatic coordination geometry; the twist angle of the two porphyrin ligands with respect to each other is approximately 30°. The deviation from an ideal square antiprism is probably due to the preferred packing orientation of the phenyl rings,

Table 2 Crystallographic data for $Th(TPP)_2 \cdot C_7H_8$, $Th(OEP)_2$, and $[Th(TPP)_2^+][SbCl_6^-] \cdot 2C_7H_8 \cdot CH_2Cl_2$.

	$C_{95}H_{64}N_8Th$	$C_{72}H_{88}N_8Th$	$C_{103}H_{74}Cl_8N_8SbTh$
space group	Fddd	$P2_1/n$	P4/nnc
T, °C	-25	28	26
a,Å	21.635(5)	15.699(1)	19.104(3)
b,Å	21.859(5)	15.474(1)	19.104(3)
c,Å	31.119(6)	26.318(2)	26.335(3)
β,°	90.59(2)	91.97(1)	90
V,Å^3	14716(5)	6389(2)	9612(5)
Z	8	4	4
mol wt	1549.6	1297.59	2061.19
d_{calcd}, g cm^{-3}	1.399	1.349	1.424
μ_{calcd},cm^{-1}	21.48	26.60	21.55
size, mm	0.2x0.2x0.2	0.4x0.4x0.5	0.3x0.3x0.4
diffractometer		Enraf-Nonius CAD4	
radiation		MoKα, λ = 0.71073 Å	
monochromator		graphite crystal, 2θ = 12°	
scan range, type		2 < 2θ < 46°, ω/θ	
scan speed, width		3-16° min, Δω = 1.50(1.00 + 0.35 tan θ)°	
rflctns, total	5547	9961	9140
rflctns, unique	5104	8889	4127
rflctns, I > 2.58 σ(I)	3646	6059	1894
internal consistency, R_i	0.026	0.031	0.020
variables	333	734	248
p factor	0.020	0.020	0.020
R_F	0.054	0.031	0.065
R_{wF}	0.069	0.038	0.106

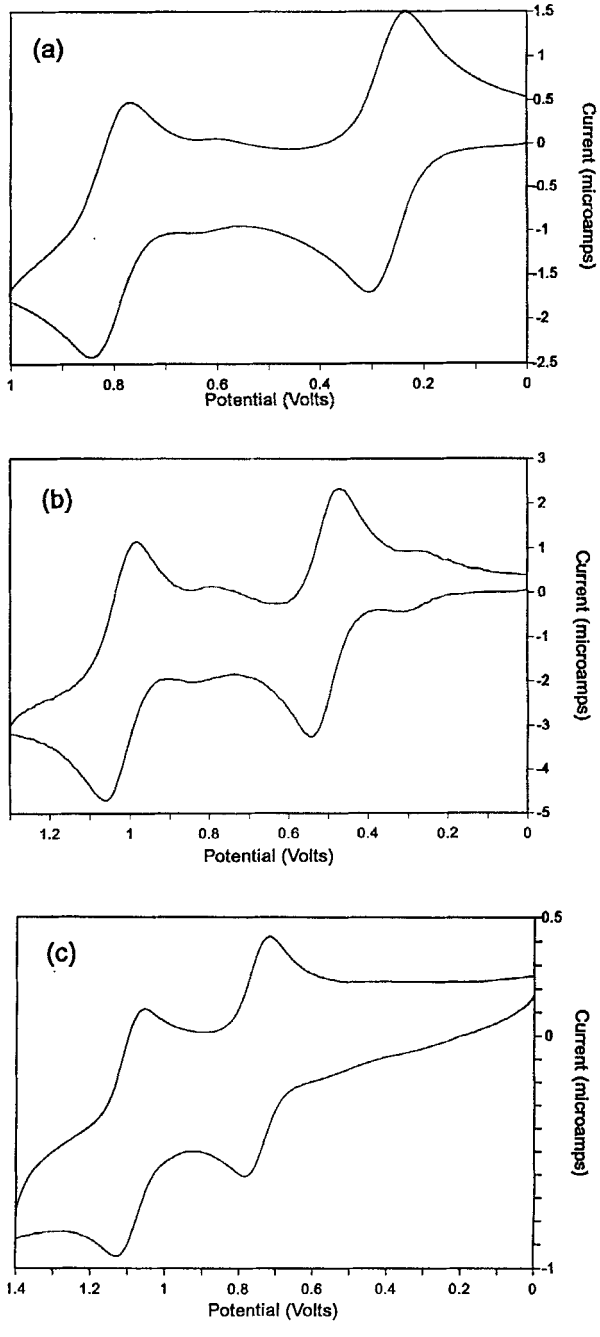

Figure 6 Cyclic voltammograms of the oxidation waves of (a) $Th(OEP)_2$, (b) Th(OEP)(TPP), and (c) $Th(TPP)_2$ in CH_2Cl_2. Potentials are relative to Ag/AgCl. The porphyrin concentrations are *ca.* 1 mM. The concentration of $[^nBu_4N][PF_6]$ was 100 mM. Scan speed = 100 mV/sec.

Table 3 Atomic coordinates for $Th(TPP)_2 \cdot C_7H_8$.

	x/a	y/b	z/c	U_{eq}[a] or U_{iso}[b]
Th	0.125	0.125	0.125	0.0217(3)
N1	0.0332(2)	0.0972(2)	0.1721(1)	0.027(3)
N2	0.0959(2)	0.0350(2)	0.0782(2)	0.029(3)
C1	0.0150(3)	0.0393(3)	0.1842(2)	0.028(4)
C2	-0.0469(3)	0.0414(3)	0.2002(2)	0.037(5)
C3	-0.0653(3)	0.0999(3)	0.1981(2)	0.034(4)
C4	-0.0160(2)	0.1352(3)	0.1808(2)	0.026(4)
C5	-0.0164(3)	0.1994(3)	0.1782(2)	0.027(4)
C6	0.0363(3)	0.0138(3)	0.0755(2)	0.026(4)
C7	0.0376(3)	-0.0514(3)	0.0714(2)	0.033(4)
C8	0.0966(3)	-0.0690(3)	0.0695(2)	0.035(4)
C9	0.1333(3)	-0.0155(2)	0.0728(2)	0.031(4)
C10	0.1976(3)	-0.0135(3)	0.0660(2)	0.028(4)
C11	-0.0774(3)	0.2302(3)	0.1836(2)	0.030(4)
C12	-0.1233(4)	0.2202(3)	0.1537(2)	0.045(4)
C13	-0.1803(4)	0.2489(4)	0.1585(3)	0.060(7)
C14	-0.1913(4)	0.2875(3)	0.1919(3)	0.052(6)
C15	-0.1465(3)	0.2975(3)	0.2215(3)	0.046(5)
C16	-0.0899(3)	0.2692(3)	0.2171(2)	0.034(4)
C17	0.2288(3)	-0.0721(3)	0.0530(2)	0.033(4)
C18	0.2729(3)	-0.0996(3)	0.0784(3)	0.047(5)
C19	0.3016(4)	-0.1535(4)	0.0654(3)	0.064(7)
C20	0.2863(4)	-0.1796(3)	0.0266(3)	0.063(7)
C21	0.2432(4)	-0.1525(4)	0.0014(3)	0.069(7)
C22	0.2138(3)	-0.0987(3)	0.0137(3)	0.049(5)
H2	-0.067(3)	0.011(3)	0.211(2)	0.04(2)
H3	-0.103(2)	0.116(2)	0.208(2)	0.04(2)
H7	0.003(2)	-0.076(2)	0.070(2)	0.03(2)
H8	0.111(2)	-0.106(2)	0.064(1)	0.02(2)
H12	-0.117(3)	0.194(2)	0.131(2)	0.06(2)
H13	-0.207(3)	0.240(3)	0.142(2)	0.04(2)
H14	-0.229(3)	0.307(3)	0.195(2)	0.05(2)
H15	-0.152(3)	0.324(3)	0.245(2)	0.05(2)
H16	-0.061(2)	0.278(2)	0.238(1)	0.02(1)
H18	0.287(3)	-0.079(3)	0.104(2)	0.05(2)
H19	0.334(3)	-0.172(3)	0.082(2)	0.06(2)
H20	0.316(3)	-0.222(3)	0.020(2)	0.09(2)
H21	0.236(3)	-0.169(3)	-0.026(2)	0.06(2)
H22	0.185(3)	-0.077(3)	-0.004(2)	0.09(3)
C23[c]	0.6783(5)	0.0689(4)	0.1153(5)	0.097(6)
C24	0.6578	0.0433	0.1538	0.121(8)
C25	0.6170	-0.0061	0.1532	0.108(7)
C26	0.5967	-0.0299	0.1140	0.071(5)
C27	0.6173	-0.0043	0.0755	0.083(5)
C28	0.6581	0.0451	0.0762	0.102(7)
C29	0.7240(8)	0.127(2)	0.1121(8)	0.146(9)

[a]Equivalent isotropic temperature factor $U_{eq} = \Sigma U_{ij}/3$.
[b]Isotropic temperature factor $U_{iso} = \exp\{-[\sin(\theta)/\lambda]^2/8\pi^2\}$.
[c]Phenyl carbon atom positions of the disordered toluene solvate were refined as a rigid group. Solvate hydrogen atoms were not included in the structure factor calculations.

Table 4 Important bond distances (Å) and angles (°) for $Th(TPP)_2 \cdot C_7H_8$.

		Distances	
Th-N(1)	2.550(9)	N(2)-C(6)	1.36(1)
Th-N(2)	2.545(9)	N(2)-C(9)	1.37(2)
Th-N(3)	2.531(10)	N(3)-C(11)	1.38(1)
Th-N(4)	2.554(9)	N(3)-C(14)	1.39(1)
N(1)-C(1)	1.37(2)	N(4)-C(16)	1.37(1)
N(1)-C(4)	1.39(1)	N(4)-C(19)	1.37(2)
		Angles	
N(1)-Th-N(1)′	109.0(3)	N(3)-Th-N(3)′	109.6(3)
N(1)-Th-N(2)	70.2(3)	N(3)-Th-N(4)	71.2(3)
N(1)-Th-N(2)′	70.6(3)	N(3)-Th-N(4)′	70.0(3)
N(1)-Th-N(3)	135.6(3)	N(4)-Th-N(4)′	109.6(3)
N(1)-Th-N(3)′	87.4(3)	Th-N(1)-C(1)	129.6(7)
N(1)-Th-N(4)	77.5(3)	Th-N(1)-C(4)	124.6(7)
N(1)-Th-N(4)′	152.4(3)	Th-N(2)-C(6)	120.9(7)
N(2)-Th-N(2)′	109.3(3)	Th-N(2)-C(9)	123.1(7)
N(2)-Th-N(3)	77.8(3)	Th-N(3)-C(11)	122.0(7)
N(2)-Th-N(3)′	151.5(3)	Th-N(3)-C(14)	123.0(7)
N(2)-Th-N(4)	87.6(3)	Th-N(4)-C(16)	126.5(8)
N(2)-Th-N(4)′	135.2(3)	Th-N(4)-C(19)	124.5(7)

since this deviation is not observed in $Th(OEP)_2$ (see below). A view of the complex from the side (Figure 7) shows that the two porphyrin rings are domed. A similar effect is observed in $Th(TPP)(acac)_2$ and is thus not due to steric repulsions between the two porphyrin rings. This doming probably helps to point the lone pairs on the porphyrin nitrogens more toward the metal, which is displaced from the central porphyrin cavity. The average Th-N distance is 2.54 Å, whereas the avereage Th-N_4 displacement is 1.46 Å. The separation between the mean N_4 planes is thus 2.92 Å.

Crystals of $Th(OEP)_2$ suitable for X-ray studies were grown by slow evaporation of a hexane solution of the porphyrin complex. This complex crystallizes in the $P2_1/n$ space group. Crystallographic data are presented in Table 2, atomic coordinates are given in Table 6, and selected bond distances and angles are collected in Table 7. In contrast to $Th(TPP)_2$, $Th(OEP)_2$ adopts a nearly perfect square antiprismatic geometry as shown in the ORTEP representation (Figure 8).

Table 5 Structural parameters of thorium porphyrin and phthalocyanine complexes.

Complex	M-N Å	M-N_4 Å	Reference
$Th(TPP)_2$	2.54	1.46	this work
$[Th(TPP)_2^+][SbCl_6^-]$	2.52	1.45	this work
$Th(OEP)_2$	2.52	1.45	this work
$[Th(TPP)(OH)_2]_3$	2.52		*a*
$Th(OEP)(acac)_2$	2.50	1.43	11
$Th(Pc)_2$[b]	2.48	1.49	*c*

[a]Kadish, K. M.; Liu, Y. H.; Anderson, J. E.; Charpin, P.; Chevrier, G.; Lance, M.; Nierlich, M.; Vigner, D.; Dormand, A.; Belkalem, B.; Guilard, R. *J. Am. Chem. Soc.*, **1988**, 110, 6455-62. [b]Pc is an abbreviation for phthalocyanine. [c]Kobayashi, T. *Bull. Inst. Chem. Res. Kyoto Univ.* **1978**, 56, 204-12.

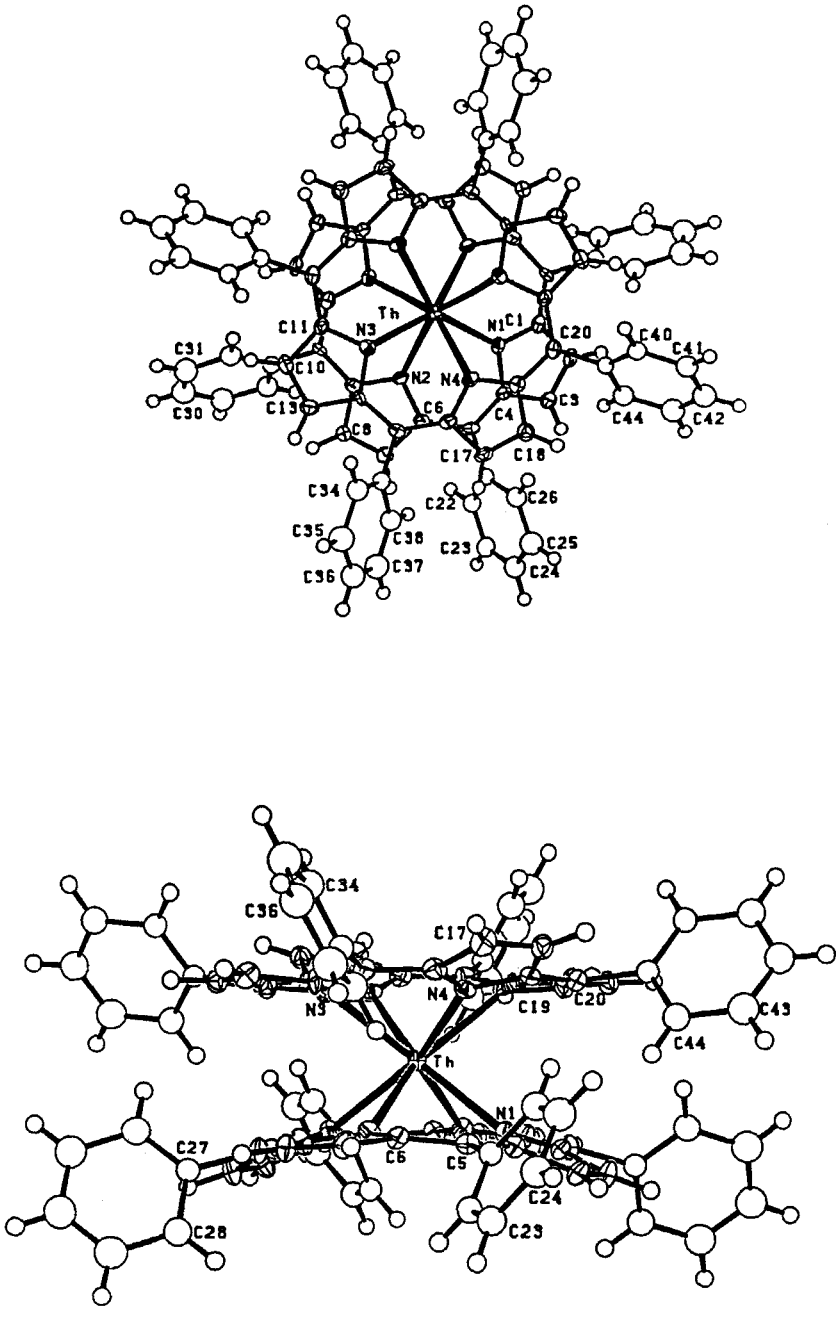

Figure 7 ORTEP diagram of $Th(TPP)_2$ viewed down the pseudo-four-fold axis (top), and viewed from the side (bottom). The 35% probability density surfaces are shown; hydrogen atoms are represented by arbitrarily-sized spheres.

Table 6 Atomic coordinates for $Th(OEP)_2$.

	x/a	y/b	z/c
Th	0.00062(1)	0.21120(1)	0.23745(1)
N1	-0.0920(3)	0.1626(3)	0.1620(2)
N2	0.0239(3)	0.0522(3)	0.2211(2)
N3	-0.0393(3)	0.1285(3)	0.3151(2)
N4	-0.1529(3)	0.2404(3)	0.2561(2)
N5	0.1062(3)	0.2284(3)	0.1675(2)
N6	0.1500(3)	0.1944(3)	0.2748(2)
N7	0.0269(3)	0.3259(3)	0.3045(2)
N8	-0.0195(3)	0.3578(3)	0.1972(2)
C1	-0.1596(4)	0.2076(4)	0.1421(2)
C2	-0.1732(5)	0.1865(5)	0.0884(3)
C3	-0.1132(5)	0.1278(5)	0.0780(2)
C4	-0.0635(4)	0.1105(4)	0.1237(2)
C5	-0.0027(4)	0.0477(4)	0.1300(3)
C6	0.0366(4)	0.0168(4)	0.1745(3)
C7	0.0885(4)	-0.0605(4)	0.1797(3)
C8	0.1040(4)	-0.0733(4)	0.2300(3)
C9	0.0617(4)	-0.0040(4)	0.2561(2)
C10	0.0539(4)	0.0032(4)	0.3089(2)
C11	0.0047(4)	0.0594(4)	0.3355(2)
C12	-0.0121(4)	0.0498(4)	0.3894(2)
C13	-0.0672(4)	0.1152(5)	0.4010(2)
C14	-0.0851(4)	0.1618(4)	0.3542(2)
C15	-0.1468(4)	0.2269(4)	0.3480(2)
C16	-0.1829(4)	0.2602(4)	0.3033(3)
C17	-0.2612(4)	0.3090(4)	0.2985(3)
C18	-0.2814(4)	0.3139(4)	0.2488(3)
C19	-0.2144(4)	0.2708(4)	0.2221(2)
C20	-0.2131(4)	0.2597(4)	0.1703(2)
C21	0.0873(4)	0.2650(4)	0.1209(3)
C22	0.1477(5)	0.2353(5)	0.0850(3)
C23	0.2044(5)	0.1837(5)	0.1088(3)
C24	0.1781(4)	0.1803(4)	0.1620(3)
C25	0.2239(4)	0.1411(4)	0.2010(3)
C26	0.2150(4)	0.1493(4)	0.2530(3)
C27	0.2750(4)	0.1195(4)	0.2921(3)
C28	0.2474(4)	0.1500(5)	0.3371(3)
C29	0.1709(4)	0.1985(4)	0.3259(3)
C30	0.1295(4)	0.2496(5)	0.3598(3)
C31	0.0670(4)	0.3110(4)	0.3514(3)
C32	0.0399(6)	0.3767(6)	0.3868(3)
C33	-0.0144(6)	0.4297(6)	0.3614(3)
C34	-0.0220(4)	0.3995(5)	0.3103(3)
C35	-0.0664(4)	0.4406(4)	0.2701(3)
C36	-0.0632(4)	0.4240(4)	0.2185(3)
C37	-0.0990(4)	0.4799(4)	0.1796(3)
C38	-0.0714(5)	0.4492(5)	0.1346(3)
C39	-0.0206(4)	0.3743(4)	0.1461(3)
C40	0.0270(5)	0.3287(5)	0.1118(3)
C41	-0.2484(7)	0.2185(6)	0.0544(3)
C42	-0.2274(8)	0.2971(9)	0.0350(5)
C43	-0.1015(6)	0.0817(6)	0.0277(3)
C44	-0.1561(8)	0.0027(7)	0.0223(4)
C45	0.1152(5)	-0.1161(5)	0.1365(3)
C46	0.1957(6)	-0.0847(6)	0.1163(3)
C47	0.1548(4)	-0.1443(4)	0.2556(3)

Table 6 Continued.

	x/a	y/b	z/c
C48	0.2424(5)	−0.1162(5)	0.2750(3)
C49	0.0205(5)	−0.0216(5)	0.4229(3)
C50	−0.0357(6)	−0.1013(5)	0.4205(3)
C51	−0.1091(5)	0.1314(6)	0.4507(2)
C52	−0.1916(6)	0.0854(7)	0.4550(4)
C53	−0.3092(5)	0.3496(6)	0.3425(3)
C54	−0.3761(8)	0.2958(8)	0.3580(5)
C55	−0.3618(4)	0.3496(5)	0.2238(3)
C56	−0.4244(5)	0.2780(6)	0.2119(4)
C57	0.1491(8)	0.2690(8)	0.0310(3)
C58	0.078(1)	0.2302(9)	−0.0014(4)
C59	0.2862(5)	0.1463(6)	0.0898(3)
C60	0.3596(6)	0.2118(7)	0.0977(5)
C61	0.3575(4)	0.0714(5)	0.2823(3)
C62	0.4298(5)	0.1326(5)	0.2719(4)
C63	0.2896(5)	0.1382(5)	0.3891(3)
C64	0.2545(7)	0.0598(7)	0.4163(3)
C65	0.0758(7)	0.3862(7)	0.4418(3)
C66	0.0241(9)	0.337(1)	0.4733(5)
C67	−0.0445(9)	0.527(1)	0.3790(6)
C68	−0.119(1)	0.503(1)	0.3890(7)
C69	−0.1544(5)	0.5570(5)	0.1884(3)
C70	−0.2436(6)	0.5338(5)	0.2036(4)
C71	−0.0848(5)	0.4875(5)	0.0817(3)
C72	−0.0149(6)	0.5509(6)	0.0693(3)

Table 7 Important bond distances (Å) and angles (°) for $Th(OEP)_2$

	Distances		
Th-N(1)	2.536(5)	N(3)-C(11)	1.373(8)
Th-N(2)	2.527(5)	N(3)-C(14)	1.376(8)
Th-N(3)	2.508(5)	N(4)-C(16)	1.377(8)
Th-N(4)	2.517(5)	N(4)-C(19)	1.376(7)
N(1)-C(1)	1.358(8)	C(1)-C(2)	1.458(9)
N(1)-C(4)	1.376(8)	C(2)-C(3)	1.34(1)
N(2)-C(6)	1.365(8)	C(3)-C(4)	1.436(9)
N(2)-C(9)	1.384(8)	C(4)-C(5)	1.369(9)
	Angles		
N(1)-Th-N(2)	70.1(2)	N(4)-Th-N(5)	141.1(1)
N(1)-Th-N(3)	109.5(1)	N(4)-Th-N(8)	79.2(2)
N(1)-Th-N(4)	71.3(1)	Th-N(1)-C(1)	124.7(4)
N(1)-Th-N(5)	80.4(1)	Th-N(1)-C(4)	123.7(4)
N(1)-Th-N(6)	140.8(2)	Th-N(2)-C(6)	124.7(4)
N(1)-Th-N(7)	146.2(2)	Th-N(2)-C(9)	124.0(4)
N(1)-Th-N(8)	83.0(2)	Th-N(3)-C(11)	125.4(4)
N(2)-Th-N(3)	75.1(1)	Th-N(3)-C(14)	124.8(4)
N(2)-Th-N(4)	110.7(1)	Th-N(4)-C(16)	125.1(4)
N(3)-Th-N(6)	83.4(1)	Th-N(4)-C(19)	126.1(4)

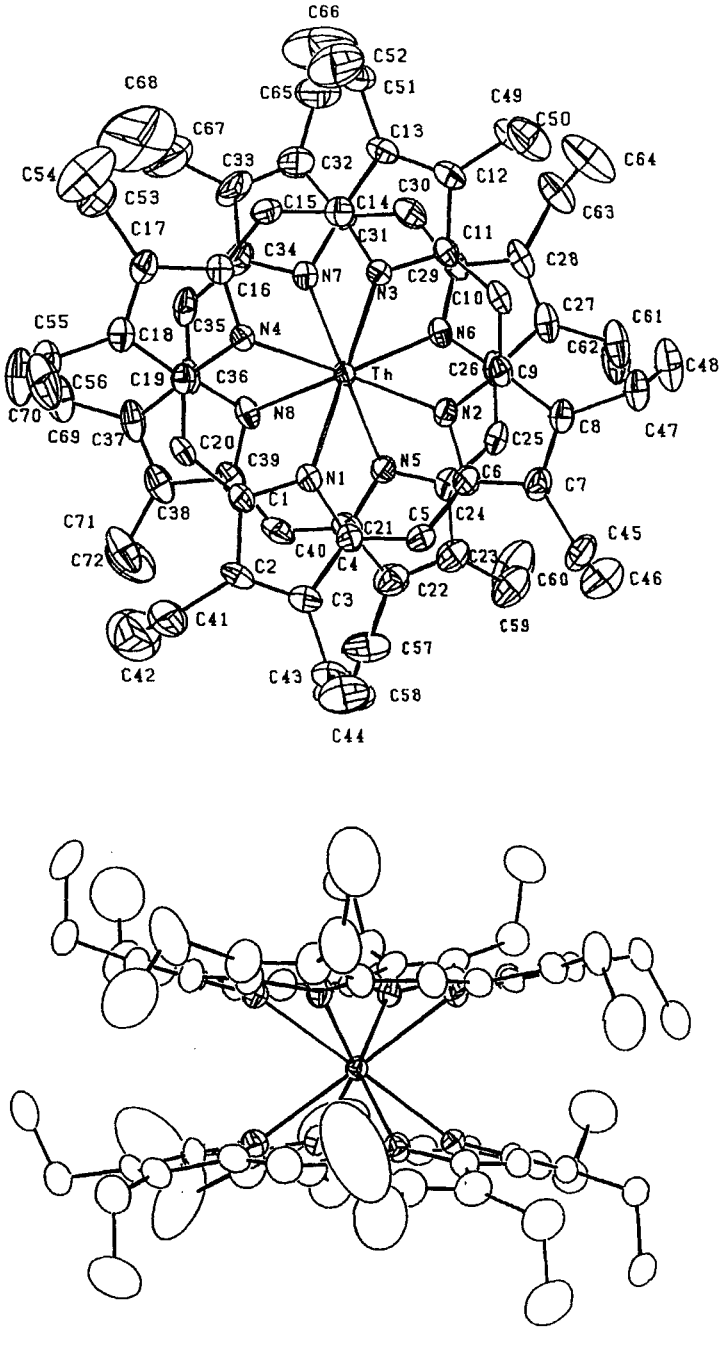

Figure 8 ORTEP diagram of $Th(OEP)_2$ viewed down the four-fold axis (top), and viewed from the side (bottom). The 35% probability density surfaces are shown.

The twist angle of the porphyrin rings with respect to each other is 42°. The average Th-N distance is 2.52 Å. The 2.89 Å separation between mean N_4 planes is slightly shorter than the 2.92 Å separation in $Th(TPP)_2$. The difference is probably ascribable to the increased interplanar steric crowding for the phenyl rings in $Th(TPP)_2$ versus the ethyl groups in $Th(OEP)_2$. The partially eclipsed porphyrin rings in $Th(TPP)_2$, which is probably a result of crystal packing effects, might also be a factor. In $Th(OEP)_2$, the perfectly staggered rings minimize steric repulsions.

Radical Cation Complexes [M(porph)$_2^+$][SbCl$_6^-$]

Treatment of the $M(TPP)_2$ or Th(TPP)(OEP) with one equivalent of phenoxathiinylium hexachloroantimonate in CH_2Cl_2 at room temperature results in the formation of the monocationic complexes $[M(TPP)_2^+][SbCl_6^-]$(M = Th or U) and $[Th(TPP)(OEP)^+][SbCl_6^-]$ after recrystallization from toluene or pentane. Elemental analyses of the products are consistent with their formulation as 1:1 hexachloroantimonate salts.

Oxidation of metalloporphyrins to π-radical cations generally results in a blue-shift of the Soret band,[13] a trend also seen in the $M(porph)_2$ cations. For $[Th(TPP)_2^+]$ and $[U(TPP)_2^+]$, the Soret band appears at 396 and 392 nm, respectively, and for $[Th(TPP)(OEP)^+]$ the Soret band is observed at 370 nm. Interestingly, the $[M(TPP)_2^+][SbCl_6^-]$ complexes exhibit a broad, intense ($\varepsilon \approx 10^3$ cm^{-1} M^{-1}), featureless absorption in the near-IR region at 1480 mm (fwhm = 300 nm) and 1270 nm (fwhm = 140 nm) for the thorium and uranium complexes, respectively. In $[Th(TPP)(OEP)^+][SbCl_6^-]$, the near-IR transition is observed at 1318 nm (fwhm = 220 nm). This spectroscopic feature, which is also seen in the oxidized photosynthetic reaction center, is characterististic of bis(porphyrin)metal π-radical cations and can be assigned to a transition from a filled porphyrin-porphyrin π-bonding orbital to the HOMO, which is a porphyrin-porphyrin π-antibonding orbital.[8a-c,e]

Porphyrin π-radical cations display IR absorptions that are not present in the unoxidized complexes.[14] These bands appear at 1297 and 1264 cm^{-1} for $[Th(TPP)_2^+]$, and at 1305, 1274, and 1266 cm^{-1} for $[U(TPP)_2^+]$; all of these new bands fall in the region diagnostic for TPP radicals (≈1300 cm^{-1}). For $[Th(TPP)(OEP)^+]$, weak cation marker bands appear at 1301 and 1274 cm^{-1}, while a very strong band is observed at 1524 cm^{-1} that falls in the region typical for OEP radicals. This therefore suggests that the unpaired electron is not fully delocalized over the two different macrocycles, but instead, the oxidation is largely centered on the OEP ring. This result is not surprising since the OEP macrocycle is significantly easier to oxidize than TPP.

The cationic thorium complexes are NMR silent in $CDCl_2$, but $[U(TPP)_2^+][SbCl_6^-]$ is easily observable by ^1H NMR spectroscopy. Evidently, the presence of the f^2 metal center provides spin-spin relaxation pathways that are not available in the thorium analogs, which render the uranium complex NMR active near 300 K. In CD_2Cl_2 at −60°C, $[U(TPP)_2^+][SbCl_6^-]$ exhibits six ^1H NMR signals that may be assigned to the pyrrole hydrogens (δ -3.48) and to the five phenyl hydrogens (δ 9.00, 8.85, 5.80, 3.82 and 0.47). The general appearance of the spectrum is similar to that of $U(TPP)_2$, except that the pyrrole signal is shifted significantly upfield. The Curie plots of the ^1H NMR chemical shifts *vs.* T^{-1} are linear (Figure 9). In the diamagnetic limit, the chemical shifts of the five different

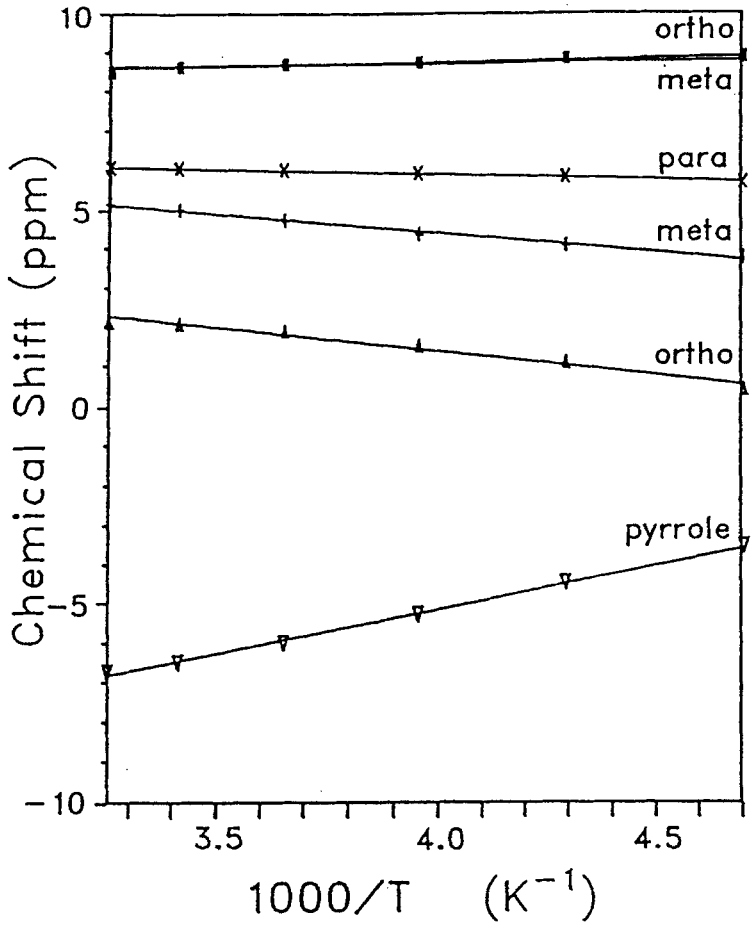

Figure 9 Curie plot of ^{1}H NMR chemical shifts of $[U(TPP)_2^+][SbCl_6^-]$ in CD_2Cl_2 *vs.* T^{-1}.

phenyl proton signals extrapolate to the normal phenyl proton region, δ 6 to 9, while the chemical shift of the pyrrole protons extrapolates to δ -14.

The oxidized complexes are EPR active in the solid state and in solution. $[Th(TPP)_2^+][SbCl_6^-]$ exhibits a sharp signal at g = 2.0029 at room temperature; the signal at 80 K is at g = 2.0016 an exhibits a peak-to-peak linewidth of 6.4 G. Similarly, $[Th(TPP)(OEP)^+][SbCl_6^-]$ exhibits a signal at g = 2.011 (linewidth = 3.16 G) at room temperature and at g = 2.010 (linewidth = 5.11 G) at 110 K. These spectra are typical of organic radicals. In contrast, the uranium complex in the solid state has no EPR signal at room temperature. At 80 K, however, two broad features are seen which sharpen dramatically upon further cooling to 7 K (Figure 10). The spectrum at 7 K has strong signals at $g_\perp = 1.343$ and $g_\parallel = 3.175$ that are characteristic of an axial system. The calculated isotropic g value of 1.953 and the large anisotropy of the g tensor ($\Delta g_{aniso} = 1.832$) suggests that the uranium center

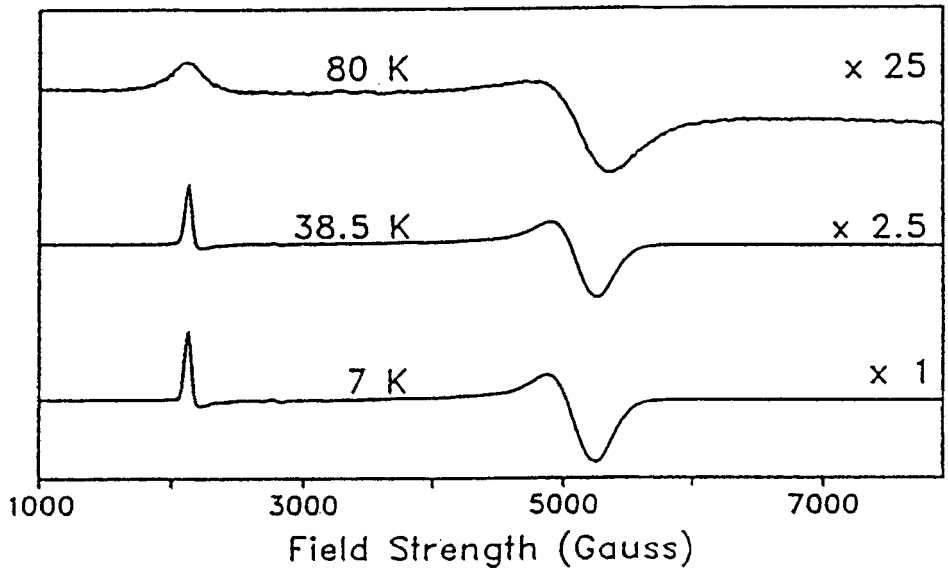

Figure 10 Solid state X-band EPR spectrum of $[U(TPP)_2^+][SbCl_6^-]$ at 80, 37.5, and 7 K.

strongly perturbs the porphyrin radical and raises the possibility that the complex at low temperature may have significant U^V character.

The magnetic susceptibility of $[Th(TPP)_2^+]$ has been determined between 4 K and 300 K (Figure 11). The magnetic moment between 200-300 K is constant with a value of $\mu_{eff} = 2.71\ \mu_B$. Between 200 K and 70 K the magnetic moment decreases to $\mu_{eff} = 1.76\ \mu_B$. The magnetic moment does not change below 70 K, and the value at these temperatures is close to the spin-only value ($1.73\ \mu_B$) for an S = 1/2 system. These values are independent of applied magnetic field. The behaviour of the magnetic moment at higher temperatures may be due to thermal population of excited states that possess f-orbital character. Such states will increase μ_{eff} above the spin-only value as a consequence of spin-orbit coupling.

SQUID magnetic susceptibility studies of solid samples of $[U(TPP)_2^+][SbCl_6^-]$ show that the magnetic moment μ_{eff} is $5.27\ \mu_B$ above 200 K (Figure 12). Between 200 K and 70 K, the value decreases to $2.20\ \mu_B$ and is constant below 70 K. Again, the values are independent of applied magnetic field. The value of μ_{eff} at low temperatures suggests that the porphyrin radical and the f^2 uranium center are antiferromagnetically coupled. Spin-orbit coupling (temperature independent paramagnetism) is probably responsible for the fact that the magnetic moment below 70 K is larger than the spin-only value expected for an S = 1/2 ground state. At higher temperature, population of the S = 3/2 excited states is probably responsible for the increase in μ_{eff}.

Crystal Structure of $[Th(TPP)_2^+][SbCl_6^-] \cdot 2C_7H_8 \cdot CH_2Cl_2$

Suitable crystals of this cation were grown under argon by layering a dichloromethane solution of $[Th(TPP)_2^+][SbCl_6^-]$ with toluene. The solvents diffused to

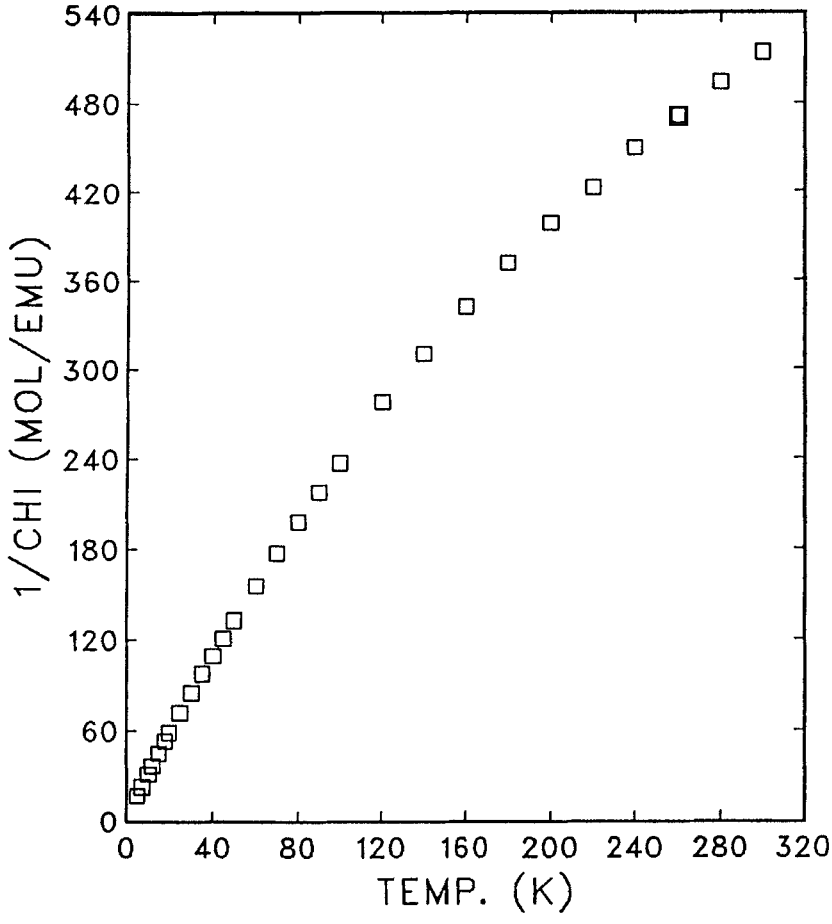

Figure 11 Plot of the temperature dependence of the reciprocal magnetic susceptibility of $[Th(TPP)_2][SbCl_6^-]\cdot C_7H_8\cdot 3CH_2Cl_2$ in an applied magnetic field of 5000 G. Between 200 and 300 K, $\theta = -146 \pm 10$ K with $c = 0.86 \pm 0.02$. Below 70 K, $\theta = -3.0 \pm 0.5$ K with $c = 0.402 \pm 0.004$.

a homogeneous mixture within four days to give large crystals. The compound crystallizes in the P4/nnc space group with one dichloromethane and two toluene solvent molecules per $[Th(TPP)_2^+][SbCl_6^-]$ unit. Crystallographic data for $[Th(TPP)_2^+][SbCl_6^-]$ are given in Table 2, while atomic coordinates and selected bond distances and angles are presented in Tables 8 and 9, respectively.

The structure of the $[Th(TPP)_2^+]$ cation is very similar to that of the neutral analog $Th(TPP)_2$. A view down the pseudo-four-fold axis (Figure 13) reveals the distorted square antiprimatic geometry of the thorium center. The twist angle between the two porphyrin ligands is approximately 30°. A view of the complex from the side (Figure 13) shows that the two porphyrin ligands are again slightly domed. The average Th-N bond length is 2.52(2) Å and the displacement of the

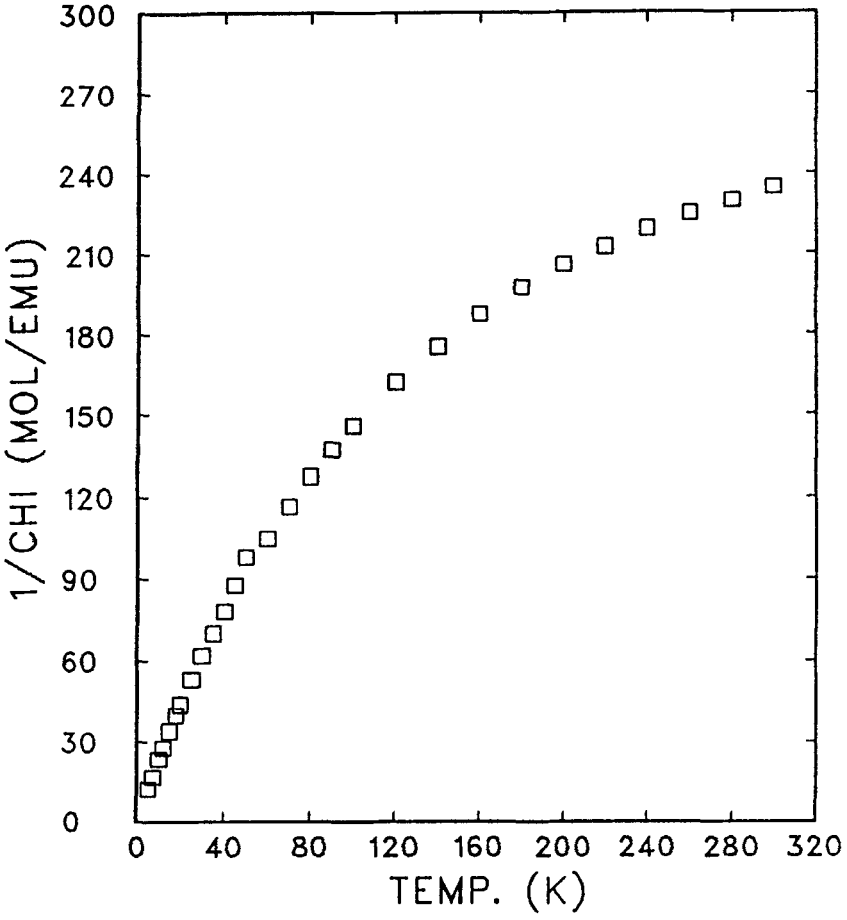

Figure 12 Plot of the temperature dependence of the reciprocal magnetic susceptibility of $[U(TPP)_2^+][SbCl_6^-]\cdot C_7H_8\cdot 3CH_2Cl_2$ in an applied magnetic field of 5000 G. Between 200 and 300 K, $\theta = -518 \pm 15$ K with $c = 3.47 \pm 0.13$. Below 70 K, $\theta = -5.3 \pm 1.4$ K with $c = 0.60 \pm 0.02$.

thorium atom from the mean N_4 plane of the porphyrin core is 1.45 Å; thus, the mean N_4 planes are separated from each other by 2.89 Å. The average Th-N bond length and Th-N_4 displacement are slightly smaller in $[Th(TPP)_2^+]$ than in $Th(TPP)_2$, where Th-N = 2.54 Å and Th-N_4 = 1.46 Å (see above). The implication of the shorter distances in the cation will be considered in the Discussion section.

Radical Dicationic Complexes, $[M(porph)_2^{2+}][SbCl_6^-]_2$

Treatment of $M(TPP)_2$ or Th(TPP)(OEP) with two equivalents of phenoxathiinylium hexachloroantimonate in dichloromethane at room temperature results in the formation of the dicationic complexes $[M(TPP)_2^{2+}][SbCl_6^-]_2$(M = Th or U) and

Table 8 Atomic coordinates for $[Th(TPP)_2^+][SbCl_6^-]\cdot 2C_7H_8\cdot CH_2Cl_2$.

	x/a	y/b	z/c
Th	0.75	0.25	0.75
Sb1	0.25	0.25	0.4821(1)
Cl1	0.25	0.25	0.5719(5)
Cl2	0.25	0.25	0.3928(5)
Cl3	0.2819(6)	0.3692(5)	0.4824(3)
N1	0.8545(9)	0.3253(9)	0.7713(6)
C1	0.876(1)	0.342(1)	0.820(1)
C2	0.950(1)	0.365(1)	0.8165(8)
C3	0.969(1)	0.360(1)	0.7656(9)
C4	0.911(1)	0.339(1)	0.7381(7)
C5	0.903(1)	0.337(1)	0.6839(9)
N2	0.7798(9)	0.3261(10)	0.6749(6)
C6	0.845(1)	0.330(1)	0.6551(9)
C7	0.842(1)	0.335(1)	0.6008(7)
C8	0.776(1)	0.336(1)	0.5880(8)
C9	0.732(1)	0.333(1)	0.6333(8)
C10	0.664(1)	0.345(1)	0.6361(9)
C21	0.971(1)	0.352(1)	0.6564(8)
C22	1.026(1)	0.301(1)	0.6581(10)
C23	1.090(1)	0.316(2)	0.631(1)
C24	1.098(2)	0.375(2)	0.601(1)
C25	1.041(2)	0.427(2)	0.6015(9)
C26	0.981(1)	0.418(2)	0.6293(9)
C27	0.624(1)	0.360(1)	0.5876(8)
C28	0.575(1)	0.316(1)	0.5691(8)
C29	0.537(1)	0.343(2)	0.525(1)
C30	0.548(2)	0.401(2)	0.499(1)
C31	0.603(2)	0.441(2)	0.519(1)
C32	0.641(1)	0.425(1)	0.5631(8)
C45	0.200(2)	0.027(3)	0.125(2)
C46	0.147	0.071	0.107
C47	0.096	0.097	0.139
C48	0.097	0.079	0.191
C49	0.149	0.035	0.209
C50	0.201	0.010	0.177
C51	0.041	0.106	0.226
C52	0.077(3)	0.167(3)	0.383(2)
C53	0.106	0.100	0.380
C54	0.088	0.056	0.340
C55	0.042	0.079	0.303
C56	0.013	0.146	0.306
C57	0.031	0.190	0.346
C58	-0.000	0.262	0.349
Cl4	0.163(5)	0.25	0.25
Cl5	0.199(3)	0.199(3)	0.25
Cl6	-0.25	-0.191(5)	0.25
Cl7	-0.196(4)	-0.196(4)	0.25
H2	0.9787	0.3793	0.8437
H3	1.0135	0.3706	0.7520
H7	0.8818	0.3379	0.5788
H8	0.7594	0.3386	0.5541
H22	1.0200	0.2589	0.6766
H23	1.1275	0.2839	0.6333
H24	1.1386	0.3819	0.5816
H25	1.0466	0.4681	0.5818
H26	0.9463	0.4537	0.6306
H28	0.5650	0.2712	0.5836
H29	0.4993	0.3147	0.5134
H30	0.5219	0.4141	0.4694
H31	0.6163	0.4825	0.5013
H32	0.6761	0.4559	0.5762

Table 9 Important bond distances (Å) and angles (°) for $[Th(TPP)_2^+][SbCl_6^-]\cdot 2C_7H_8\cdot CH_2Cl_2$.

	Distances		
Th-N(1)	2.52(2)	C(3)-C(4)	1.38(3)
Th-N(2)	2.52(2)	C(4)-C(5)	1.43(5)
N(1)-C(1)	1.38(3)	C(5)-C(6)	1.35(3)
N(1)-C(4)	1.41(3)	C(6)-C(7)	1.43(3)
N(2)-C(6)	1.35(3)	C(7)-C(8)	1.31(3)
N(2)-C(9)	1.43(3)	C(8)-C(9)	1.46(3)
C(1)-C(2)	1.48(4)	C(9)-C(10)'	1.33(3)
C(2)-C(3)	1.39(3)	C(1)-C(10)'	1.39(4)
	Angles		
N(1)-Th-N(1)'	154.3(5)	N(2)-Th-N(2)'	76.6(6)
N(1)-Th-N(1)''	110.5(5)	N(2)-Th-N(2)''	109.6(6)
N(1)-Th-N(1)'''	75.4(1)	N(2)-Th-N(2)'''	153.8(6)
N(1)-Th-N(2)	70.6(5)	Th-N(1)-C(1)	125(1)
N(1)-Th-N(2)'	133.0(5)	Th-N(1)-C(4)	125(1)
N(1)-Th-N(2)''	71.1(5)	Th-N(2)-C(6)	123(1)
N(1)-Th-N(2)'''	88.6(5)	Th-N(2)-C(9)	121(1)

$[Th(TPP)(OEP)^{2+}][SbCl_6^-]_2$. The bis-TPP products can be isolated as dark purple-black microcrystals by collecting the precipitated solid and washing with CH_2Cl_2, while $[Th(TPP)(OEP)^{2+}][SbCl_6^-]_2$ can be recrystallized from CH_2Cl_2/toluene. A slight deficiency of the oxidant is used in the preparation of the bis-TPP complexes since it is difficult to separate the desired products from excess oxidant.

All of the dicationic sandwich complexes exhibit a blue-shift of the near-IR absorption relative to the analogous monocations. For $[Th(TPP)_2^{2+}]$ and $[U(TPP)_2^{2+}]$, the broad absorptions are observed at 1080 nm (fwhm = 190 nm) and 900 nm (fwhm = 200 nm), respectively, while $[Th(OEP)(TPP)^{2+}]$ displays a broad, featureless band at 956 nm (fwhm = 160 nm).

In general, oxidation of a monocationic sandwich compound to the corresponding dication results in a blue-shift of the Soret band.[13] This is seen in $[Th(OEP)(TPP)^{2+}]$, which displays a Soret band at 364 nm (*vs.* 370 nm in $[Th(OEP)(TPP)^+]$ and 393 nm in Th(OEP)(TPP)). In contrast, the Soret absorptions in the $M(TPP)_2^{2+}$ complexes are *red-shifted* relative to those of the monocations, and appear at 397 and 396 nm in the thorium and uranium complexes, respectively.

The IR spectrum of $[Th(TPP)_2^{2+}]$ has strong bands at 1285 and 1267 cm^{-1} not found for $Th(TPP)_2$, and the spectrum of $[U(TPP)_2^{2+}]$ has bands at 1295, 1287, and 1269 cm^{-1} not found for $U(TPP)_2$. The new bands are more intense than those of the mono-oxidized complexes but are in similar locations; they are in the correct location to be radical cation "marker" bands.[14] For $[Th(OEP)(TPP)^{2+}]$, the marker bands appear at 1533, 1328, 1302, and 1276 cm^{-1}. Again, the OEP marker band at 1533 cm^{-1} is much more intense than the TPP marker bands near 1300 cm^{-1}.

The dicationic complexes are NMR active. The proton NMR spectrum of $[Th(TPP)_2^{2+}][SbCl_6^-]_2$ at 18 °C in CD_3CN consists of three broad overlapping signals and two well separated signals (Figure 14). Deconvolution of the overlapping signals reveals that the spectrum consists of five signals of equal intensity due to the phenyl group (δ 7.55, 7.47, 7.37, 6.98, and 6.30); the pyrrole signal is missing. Two explanations are plausible. First, the complex is paramagnetic (S = 1 ground state)

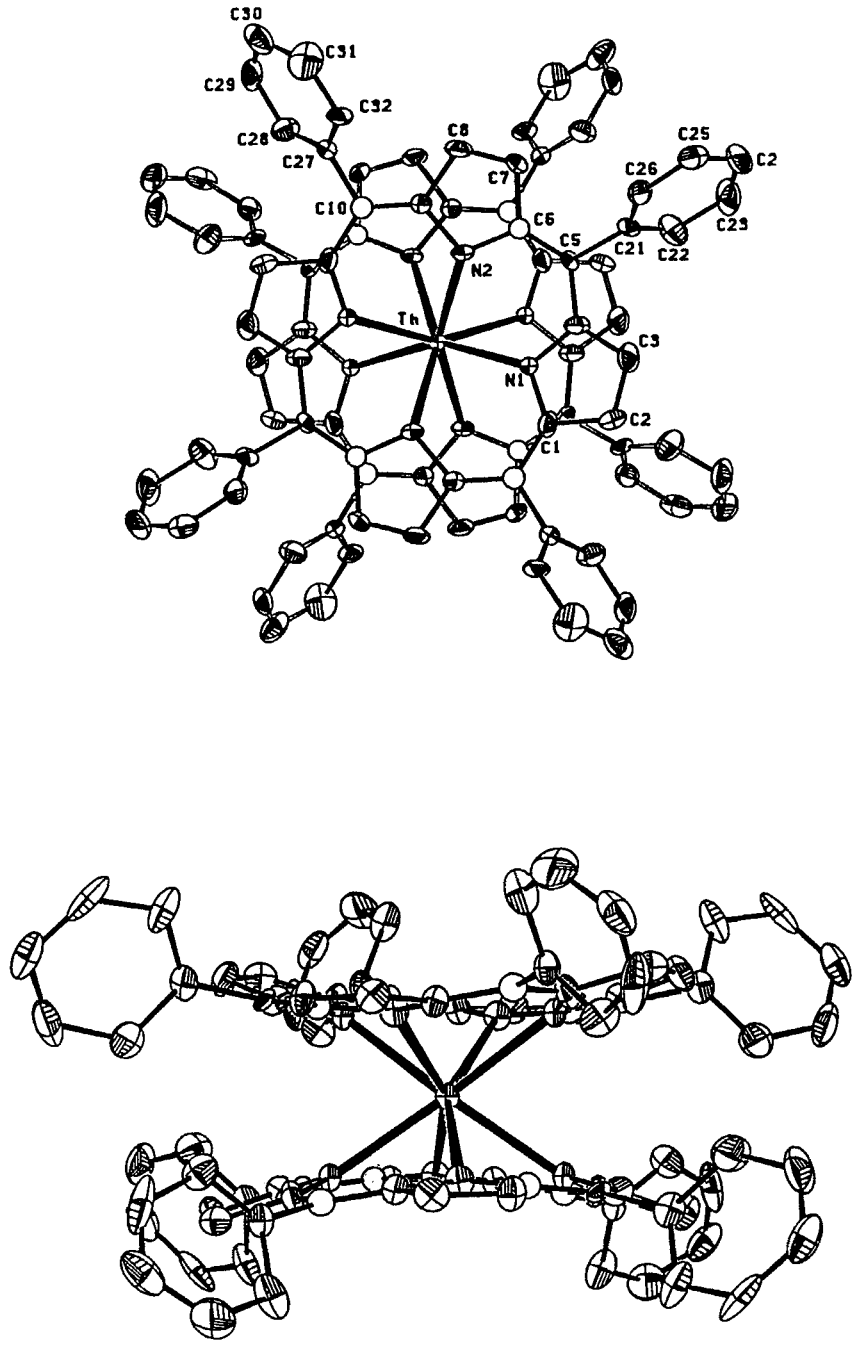

Figure 13 ORTEP diagram of $[Th(TPP)_2^+]$ viewed down the four-fold axis (top), and viewed from the side (bottom). The 35% probability density surfaces are shown.

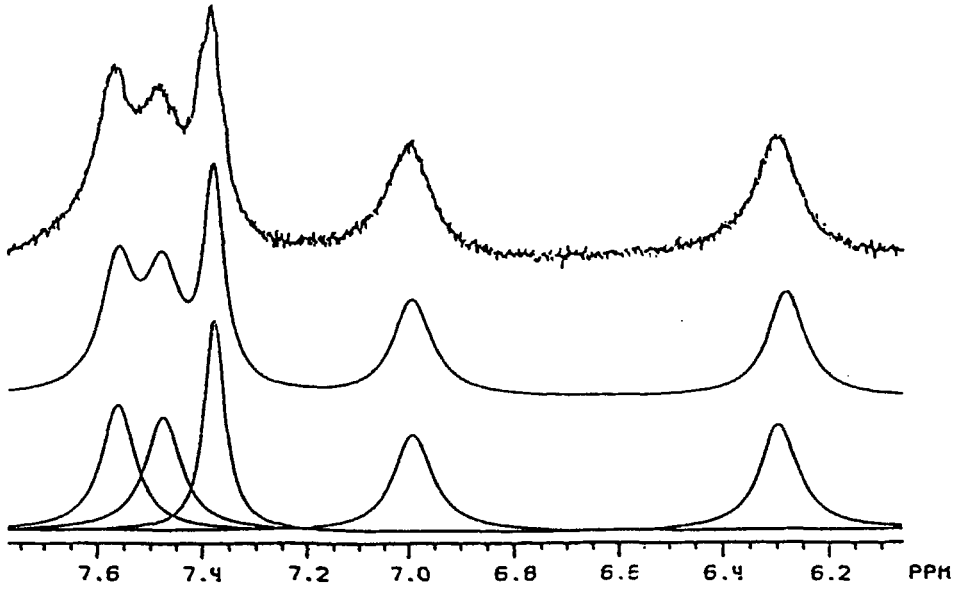

Figure 14 360 MHz ^{1}H NMR spectrum of $[Th(TPP)_2^{2+}][SbCl_6^-]_2$ in CD_3CN: actual spectrum (top), deconvoluted spectrum (middle), and five Lorentzian components of the deconvoluted spectrum (bottom).

but the unpaired electrons do not affect the NMR signals of protons that are far from areas of spin density, such as the protons on the phenyl rings. This explanation, however, seems unlikely since the phenyl chemical shifts are in the normal chemical shift region. Furthermore, the chemical shifts are not temperature-dependent as would be expected of a paramagnetic molecule. An alternative explanation is that $[Th(TPP)_2^{2+}]$ is diamagnetic (S = 0 ground state) but the ^{1}H NMR spectrum is affected by intermolecular electron transfer with monocationic $[Th(TPP)_2^+]$ impurities in solution. It has been demonstrated that solutions of the dicationic complex contain small amounts (<5%) of the monocationic complex (see below). The effect of this self-exchange process is dramatic because the monocationic complex is a paramagnetic species. The large linewidths of the phenyl signals and the absence of the pyrrole signal are understandable since the pyrrole protons would be broadened the most by the presence of unpaired electron density in the porphyrin π-system. The ^{1}H NMR spectrum of $[Th(OEP)(TPP)^{2+}]$ is essentially identical to that of Th(OEP)(TPP).

The proton NMR spectrum of $[U(TPP)_2^{2+}][SbCl_6^-]_2$ at 20 °C in CD_3CN consists of six signals due to the pyrrole (δ 4.15) and phenyl protons (δ 8.40, 7.56, 5.95, 4.88, and -1.73). The chemical shifts of the phenyl protons are linearly related to T^{-1} as illustrated in the Curie plot (Figure 15). In the diamagnetic limit, the phenyl and pyrrole proton signals collapse to their normal range of 6-10 ppm; this behavior is unlike that of $[U(TPP)_2^+]$, since the pyrrole protons of the monocation extrapolate to negative chemical shifts in the diamagnetic limit. The resemblance of the NMR spectrum of $[U(TPP)_2^{2+}]$ to that of $U(TPP)_2$ suggests that, as in the case in the neutral molecule, there are no unpaired electrons in the porphyrin π-system

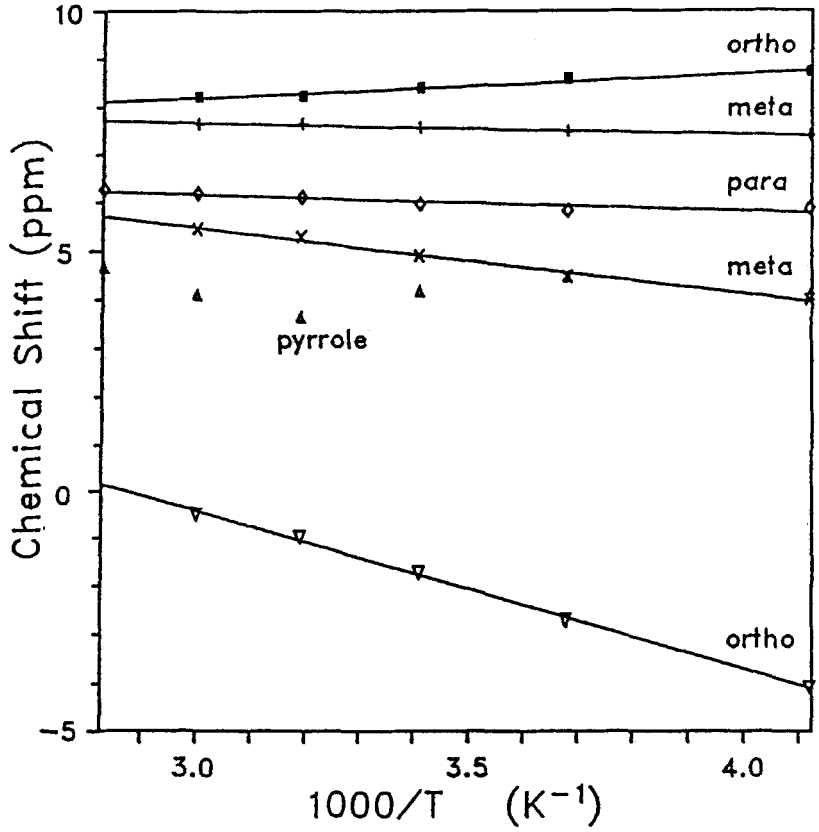

Figure 15 Curie plot of chemical shifts of $[U(TPP)_2^{2+}][SbCl_6^-]_2$ in CD_3CN *vs.* T^{-1}.

of the dication and that the ^1H NMR shifts are only affected by the two f-electrons on the uranium center.

None of the dications is EPR active either at room temperature or at 77 K, although the presence of a trace amount of the monocation $[Th(TPP)_2^+][SbCl_6^-]$ is evident in the $[Th(TPP)_2^{2+}][SbCl_6^-]_2$ sample. The impurity concentration is approximately 5% as estimated by comparison of the intensity of the EPR signal with that of a bonafide sample of $[Th(TPP)_2^+][SbCl_6^-]$.

DISCUSSION

Synthetic Route

The synthesis of bis(porphyrinato)thorium(IV) and -uranium(IV) complexes from the corresponding metal tetrakis(dialkylamide) complexes and freebase porphyrin is straightforward and occurs in high yield. The products are the first bis(porphyrinato)actinide complexes to be prepared.[3] The advantages of using homoleptic metal amide starting materials are that the reaction temperatures are low, no redox

chemistry occurs, and the reaction solutions are non-acidic. This synthetic route should work for any metal that forms amide complexes and for any porphyrin which does not have functional groups that are susceptible to attack by amide ions or amines.

Electronic Structure of the M(porph)$_2$ Complexes

The spectroscopic features of the M(porph)$_2$ complexes provide important insights into the electronic structures of these species. One of the characteristic properties of the M(porph)$_2$ complexes is that the Soret bands are blue-shifted relative to those of analogous mono(porphyrin) complexes. Similar blue-shifted Soret bands are present in the zinc face-to-face porphyrin complex (Zn_2FTF_4) synthesized by Collman[15] and in other closely spaced bis(porphyrin) complexes.[16] The unusual shift of the Soret band in these complexes has been attributed to excitonic coupling between the two closely-spaced porphyrin π systems.

The other characteristic spectroscopic feature of dimeric porphyrin complexes is the presence in oxidized systems of near-IR absorptions at approximately 1000 nm. For the actinide sandwich complexes this absorption appears at *ca.* 1400 nm in the [M(porph)$_2^+$] cations and *ca.* 1000 nm in the [M(porph)$_2^{2+}$] dications. For the lanthanide and transition metal bis(porphyrin) complexes, this band is shifted to higher energy due to the increased overlap between the porphyrin rings. Buchler has discussed the near-IR absorption of the neutral M(porph)$_2$ complexes (where M is a trivalent lanthanide metal) as an intramolecular ring-to-ring electron transfer from the HOMO of the porphyrin mono-anion-radical (porph^{1-}) to the LUMO of the dianionic porphyrin (porph^{2-}).[2] Implicit in this proposal is the assumption that the porphyrin-porphyrin interaction is weak.

More recently, however, a molecular orbital model of bis(porphyrin) systems has been developed that more satisfactorily accounts for the spectroscopic features of such systems than does the excitonic coupling model or Buchler's intramolecular electron transfer hypothesis. Bocian has proposed that the strong π-π interactions present give rise to a new set of bonding and antibonding "supermolecular" molecular orbitals.[8] Thus, in the M(TPP)$_2$ complexes, the filled a_{2u} HOMO's of each individual porphyrin ring interact to give a bonding a_{1u} MO and an antibonding a_{1u}* MO, as shown in Figure 16. For the M(OEP)$_2$ case, a similar scheme is applicable, except the constituent HOMO's are of a_{2u} symmetry. In the neutral complexes, both new "supermolecular" MO's are filled; oxidation removes an electron from the porphyrin-porphyrin antibonding orbital. In support of this model, the spacing between porphyrin rings in Th(TPP)$_2$ *decreases* upon oxidation to [Th(TPP)$_2^+$]: 2.92 Å *vs* 2.89 Å. This structural change is consistent with the loss of a porphyrin-porphyrin antibonding electron upon formation of the cationic complex. A weak multi-center π-bond is thus formed between the two porphyrin macrocycles.

The antibonding nature of the HOMO is also reflected in the redox potentials of Th(TPP)$_2$, since this complex is much easier to oxidize than is the monoporphyrinic complex Th(TPP)(acac)$_2$.[11b] The analogous uranium complex, U(TPP)$_2$, is even easier to oxidize than Th(TPP)$_2$, which suggests that there is more antibonding character to the HOMO in U(TPP)$_2$. This observation reflects the closer spacing of the porphyrin units in this complex, since the ionic radius of U^{IV} of 0.97 Å is smaller than the ionic radius of Th^{IV} of 1.02 Å. The trend is continued for Ce, Zr,

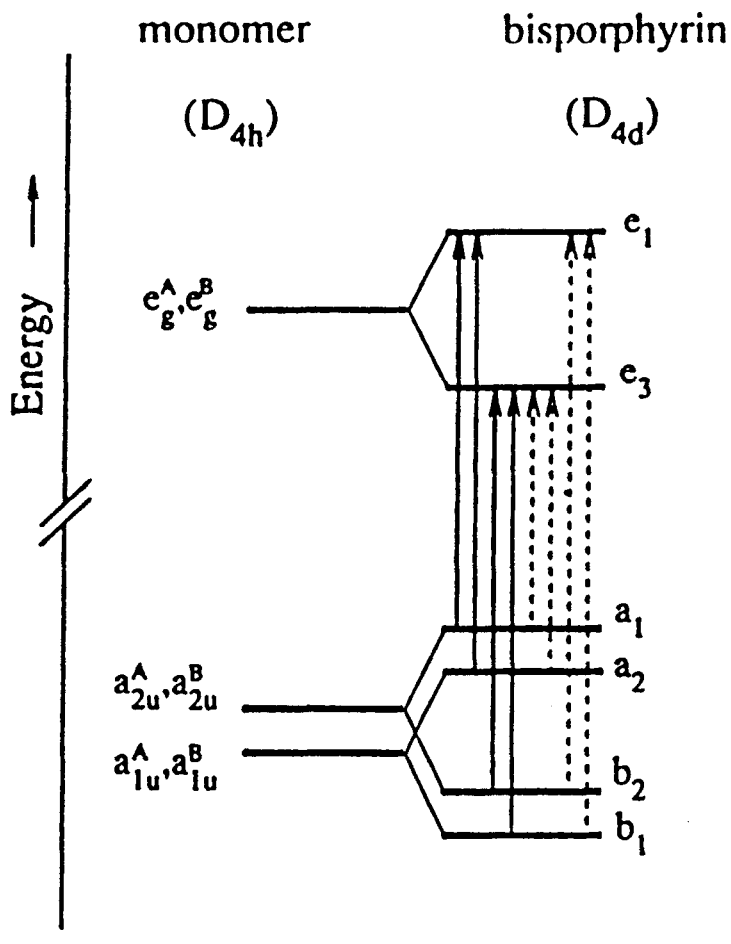

Figure 16 Schematic diagram of the "supermolecular" MO model. Allowed transitions are denoted by solid arrows and forbidden transitions by dashed arrows. Adapted from ref 9e.

Table 10 Oxidation potentials and cation near-IR absorption for $M(TPP)_2$ complexes.

Complex	$oxidn_2$	$oxidn_1$	NIR	Ref.
$Th(TPP)_2$	1089	741	1480	this work
$Ce(TPP)_2$	1078	664	1350	2c, 2e
$U(TPP)_2$	1060	625	1270	this work
$Zr(TPP)_2$	984	522	1074	4a, 4c, 4d
$Hf(TPP)_2$	989	531	1054	4c, 4d

All potentials measured in mV in CH_2Cl_2 vs. Ag/AgCl. $FeCp_2$ oxidation occurs at 510 mV under these conditions. Near-IR band of cations measured in CH_2Cl_2.

and Hf bis(porphyrin) complexes; as the metal radius decreases, the oxidation potentials also decrease (Table 10). For Th(OEP)(TPP), the redox potentials depend on both the interplanar separation *and* on the energy difference between molecular orbitals of the individual porphyrin macrocycles.

Investigation of the oxidized analogs $[M(TPP)_2^+][SbCl_6^-]$ and $[M(TPP)_2][SbCl_6]_2$ has further broadened our understanding of the electronic interactions operative in this class of complexes. As judged by EPR spectroscopy, the monocations $[Th(TPP)_2^+]$ and $[Th(OEP)(TPP)^+]$ are "simple" organic radicals with a half-filled HOMO containing one unpaired electron in the π-system. In contrast, the uranium complex $[U(TPP)_2^+][SbCl_6^-]$ is EPR silent at 300 K and only gives an EPR spectrum below 80 K; the spectrum at 7 K appears to be that of an axially symmetric complex with $g_{\|} = 3.175$ and $g_{\perp} = 1.343$. The large anisotropy of the g-tensor is strong evidence that uranium f-electrons are interacting with the porphyrin π-system.

Oxidation of the sandwich complexes also gives rise to a new electronic transition between the filled "supermolecular" bonding MO and the now half-full antibonding MO. This transition is observed in the near-IR and increases in energy with decreasing porphyrin-porphyrin separation, since the energy gap between bonding and antibonding "supermolecular" orbitals increases as the interplanar π-π interactions increase. Thus, the near-IR band energy increases as the metal is changed in the order Th>Ce>U >Zr>Hf (Table 10). Removal of a second electron from the π-system results in dicationic complexes, in which the net antibonding interaction decreases by one additional electron. This leads to even stronger π-π interactions than in the monocations, and results in a larger energy gap between the "supermolecular" bonding MO and the now empty antibonding MO. This is supported by the observed blue-shift in the near-IR band upon formation of the dications.

The doubly-oxidized complexes $[Th(TPP)_2^{2+}][SbCl_6^-]_2$ and $[U(TPP)_2^{2+}][SbCl_6^-]_2$ are EPR silent but are NMR active at 300 K. The dicationic thorium complex, $[Th(TPP)_2^{2+}]$, appears to be diamagnetic since the proton NMR signals are temperature independent. The diamagnetism of $[Th(TPP)_2^{2+}]$ and $[Th(OEP)(TPP)^{2+}]$ is consistent with removal of two electrons from the porphyrin-porphyrin antibonding HOMO. The properties of the dicationic uranium complex, $[U(TPP)_2^{2+}]$, also support this conclusion. The temperature dependence of the ^1H NMR chemical shifts of $[U(TPP)_2^{2+}]$ is quite similar to that of the analogous neutral precursor, $U(TPP)_2$. This resemblance suggests that, as for the neutral molecule, there are no unpaired electrons in the porphyrin π-system of $[U(TPP)_2^{2+}]$ and that the ^1H NMR chemical shifts are only affected by the two f-electrons on the uranium center.

As mentioned earlier, new absorptions are observed in the visible spectra of the unoxidized bis(porphyrin)metal complexes which are not seen in monoporphyrin complexes. Holten and coworkers have investigated the origin of these transitions and have found that they are due predominantly to charge resonance states arising from the substantial porphyrin-porphyrin interactions present.[9c-e] Also observed in the sandwich complexes are new excited states not seen in monoporphyrins. We have previously reported studies of the luminescence of $Th(OEP)_2$ from an unusually low energy $^1(\pi,\pi^*)$ excited state which also arises from charge resonance states due to the strong π-π interactions present.[9c]

Strong π-π interactions like those discussed above are not unique to *synthetic* metalloporphyrin complexes. Buchler noted that the electron deficient neutral

$M(porph)_2$ complexes of trivalent lanthanide ions and the oxidized $[M(porph)_2^+]$ complex of Ce are spectroscopically similar to the "special pair" of Rhodopseudomonas viridis,[2,6] in which two bacteriochlorphyll units are held in a dimeric arrangement. In light of the preceding discussion regarding the electronic structure of $M(porph)_2$ complexes, it appears reasonable to suggest that the "special pair" is dimeric to lower its oxidation potential and to lengthen the lifetime of its photoexcited states. The lower oxidation potential and long-lived triplet excited states should improve the rate and/or efficiency of the photoionization process and thereby enhance the photosynthetic generation of reducing equivalents.

EXPERIMENTAL

All procedures were carried out under an argon atmosphere except where otherwise stated. The solvents used were reagent grade and were distilled from sodium/benzophenone (pentane, diethyl ether, benzene, tetrahydrofuran, 1,2-dimethoxyethane), sodium (toluene, heptane), or calcium hydride (acetonitrile, benzonitrile, dichloromethane) before use. The reagents UCl_4,[17] H_2TPP,[18] H_2OEP,[19] and $[C_{12}H_8OS][SbCl_6]$[20] were prepared *via* literature routes. Thorium tetrachloride was purchased from Cerac and used as received.

Elemental analyses were performed by Mr. Tom McCarthy of the School of Chemical Sciences Microanalytical Laboratory at the University of Illinois, and mass spectroscopic studies were performed by Dr. Richard Milberg or Mr. Steve Mullen of the School of Chemical Sciences Mass Spectroscopy Laboratory at the University of Illinois. UV-Visble spectra were recorded on an IBM 9430 spectrophotometer; UV-Vis-NIR spectra were recorded on a Varian 2300 spectrophotometer. Infrared spectra were recorded on a Perkin Elmer 1600 or 1750 Fourier transform spectrophotometer as Nujol mulls between KBr plates. Cyclic voltammetric studies were performed using a BAS-100 potentiostat with a Pt disc working electrode and a Ag/AgCl reference electrode. The locations of the redox processes were calibrated relative to the ferrocene/ferrocenium couple at 0.510 V *vs.* Ag/AgCl in methylene chloride. The supporting electrolyte used in all experiments was $[^nBu_4N][PF_6]$, which was recrystallized from ethanol prior to use. ^1H NMR spectra at 300 and 360 MHz were recorded on a General Electric QE-300 or a Nicolet NT-360 Fourier transform spectrometer. Chemical shifts are reported in δ units and are uncorrected for the paramagnetic shift of the reference, if any. X-band EPR spectra were recorded at room temperature, 110 K, and 77 K on a Varian E-9 or Bruker ESP-300 spectrometer, and at 80 K, 38.5 K, and 7 K on a Bruker ER 200D-SRC spectrometer.

Thorium Tetrachloride Tris-tetrahydrofuran, $ThCl_4(thf)_3$

Anhydrous $ThCl_4$ (100 g, 0.27 mol) was extracted in a Soxhlet apparatus with tetrahydrofuran (400 mL) for one week. The resulting brown solution was filtered from some off-white solid and cooled to −20°C for four days. The resulting crystals were collected and dried under vacuum at 75°C for 48 h to give $ThCl_4(thf)_3$ as an off-white powder. A second crop of crystals may be collected by concentration

of the mother liquor. Yield: 130 g (83 %). Calcd. for $C_{12}H_{24}O_3ThCl_4$: C, 24.4; H, 4.1; Th, 39.3; Cl, 24.0. Found: C, 25.1; H, 4.5; Th, 38.7; Cl, 22.8.

Tetrakis(diethylamido)uranium(IV), $U(NEt_2)_4$

The complex $U(NEt_2)_4$ was made by a modification of the literature route from $LiNEt_2$ and UCl_4.[21] Diethyl ether (40 mL) was condensed onto a mixture of UCl_4 (1.02 g, 2.7 mmol) and $LiNEt_2$ (0.86 g, 10.9 mmol) at −196°C. The mixture was warmed to room temperature and stirred for 12 h. The green-black solution was filtered from a small amount of insoluble material and the volatile material was removed under vacuum. The residue was extracted with pentane (20 mL) and the solution was filtered. The pentane solution was used immediately.

Tetrakis(diethylamido)thorium(IV), $Th(NEt_2)_4$

This complex was made by a modification of the literature route from $LiNEt_2$ and $ThCl_4(thf)_3$.[22] Diethyl ether (40 mL) was condensed at −196°C onto a mixture of $ThCl_4(thf)_3$ (1.01 g, 1.7 mmol) and $LiNEt_2$ (0.57 g, 7.2 mmol). The mixture was warmed to room temperature and stirred for 24 h. The brown solution was filtered from a small amount of insoluble material and taken to dryness under vacuum. The residue was extracted with pentane (20 mL) and the solution was filtered. The pentane solution was used immediately.

Tetrakis(dimethylamido)thorium(IV), $Th(NMe_2)_4$

This complex was made by a modification of the literature route from $LiNMe_2$ and $ThCl_4(thf)_3$.[22] Diethyl ether (80 mL) was condensed at −196°C onto a mixture of $LiNMe_2$ (0.51 g, 10.0 mmol) and $ThCl_4(thf)_3$ (1.44 g, 2.45 mmol) and the mixture was warmed to room temperature and stirred for 24 h. The ether solution was filtered and was taken to dryness under vacuum. The solid obtained was extracted with pentane (50 mL) and the filtered extract was taken to dryness to give $Th(NMe_2)_4$ as a cream-colored solid. The yield for this reaction is typically 30 to 50%.

Bis(tetraphenylporphyrinato)uranium(IV), $U(TPP)_2$

To H_2TPP (5.0 g, 8 mmol) in toluene (150 mL) was added $U(NEt_2)_4$ (4 mmol) in pentane (15 mL). The reaction mixture was stirred at 20°C for 7 days, and then heated to reflux for 12 h. After being cooled, the mixture was opened to air, transferred (both solid and liquid) into a large Erlenmeyer flask, diluted with toluene (2 L), and stirred overnight. The resulting purple precipitate was collected by filtration, washed with toluene until the washings were colorless (*ca.* 500 mL), and lastly, washed with pentane (100 mL). The material was air dried at room temperature to give crude $U(TPP)_2$. Yield 3.8 g (62%). The toluene supernatant from the above operation contains unreacted H_2TPP.

Crude $U(TPP)_2$, free of H_2TPP, was further purified in batches by chromatography on a wet packed silica gel (0.2-0.05 mm) column using $CHCl_3$ as eluent. $U(TPP)_2$ (0.5g) dissolved in $CHCl_3$ (50 mL) was loaded in a 2-3 cm band on the top of a 7.5 × 20 cm column of silica gel. The product eluted first as a diffuse

brown-black band approximately 6 cm in height which required about 300 mL of eluent. A small amount of dark material remained at the top of the column and two slow moving bands, one very sharp, the second 2-3 cm wide, were abandoned on the column. The chloroform solution was concentrated to about 50 mL using a rotary evaporator, filtered through an ultra-fine glass frit, transferred to a Schlenk flask, and taken to dryness to give $U(TPP)_2$. Yield: 0.34 g (68%). *Anal.* Calcd. for $C_{88}H_{56}N_8U$: C, 72.2; H, 3.9; N, 7.7; U, 16.3. Found: C, 72.4; H, 3.8; N, 7.6; U, 15.6. UV-Vis($CHCl_3$, nm): 404 (Soret), 485, 550. FAB MS: parent ion envelope at m/z 1464.7. ^1H NMR ($CDCl_3$, −20°C): δ 10.42 (d, J_{HH} = 6.9 Hz, o-H), 7.21 (t, J_{HH} = 7.4 Hz, m-H), 5.34 (t, J_{HH} = 7.1 Hz, p-H), 3.76 (s, fwhm = 8 Hz, pyrrole-H), 3.18 (t, J_{HH} = 7.4 Hz, m-H), −6.13 (s, fwhm = 16 Hz, o-H). IR(cm^{-1}): 3100 w, 3079 w, 3050 w, 3022 w, 2721 w, 2692 w, 2621 w, 2531 w, 2488 w, 2409 w, 2359 w, 2388 w, 2223 w, 2164 w, 1956 w, 1894 w, 1824 w, 1800 w, 1775 w, 1640 w, 1596 s, 1574 m, 1542 w, 1523 m, 1495 sh, 1481 sh, 1441 sh, 1327 s, 1225 m, 1195 m, 1180 m, 1156 m, 1071 s, 1033 w, 1004 s, 981 s, 921 m, 901 m, 853 w, 800 s, 759 s, 750 s, 726 s, 703 s, 670 w, 657 m, 636 m, 636 w, 622 m, 579 m, 526 m, 498 w, 465 m, 428 m.

Bis(tetraphenylporphyrinato)thorium(IV), $Th(TPP)_2$

To H_2TPP (5.0 g, 8.1 mmol) slurried in toluene (150 mL) was added $Th(NEt_2)_4$ (4 mmol) dissolved in pentane (20 mL). The mixture was stirred for 7 days and then heated to reflux for 12 h. The reaction mixture was subsequently treated as described for the uranium complex (see above). Yield before chromatography: 2.8 g (47%). The crude material may be purified by chromatography on silica gel by following the procedure described above. *Anal.* Calcd. for $C_{88}H_{56}N_8Th$: C, 72.5; H, 3.9; N, 7.7; Th, 15.9. Found: C, 72.6; H, 3.8; N, 7.6; Th, 15.5. UV-Vis ($CHCl_3$, nm): 402 (Soret), 553. FD MS: parent ion envelope at m/z 1456.5. ^1H NMR ($CDCl_3$, −20 °C): δ 9.33 (d, J_{HH} = 7.5 Hz, o-H), 8.32 (s, fwhm = 5 Hz, pyrrole), 8.06 (t, J_{HH} = 7.7 Hz, m-H), 7.73 (t, J_{HH} = 7.6 Hz, p-H), 7.27 (t, J_{HH} = 7.6 Hz, m-H), 6.57 (d, J_{HH} = 7.5 Hz, o-H). IR (cm^{-1}): 3100 w, 3056 w, 3018 w, 2725 w, 2692 w, 2617 w, 2530 w, 2481 w, 2360 w, 2336 w, 2163 w, 1956 w, 1891 w, 1813 w, 1692 w, 1596 m, 1574 w, 1537 w, 1519 w, 1494 sh, 1340 sh, 1326 m, 1226 w, 1197 m, 1180 m, 1156 w, 1071 m, 1034 w, 1005 s, 983 s, 926 w, 878 w, 851 w, 832 w, 800 s, 758 s, 751 s, 722 s, 703 s, 670 w, 658 w, 636 w, 622 m, 579 m, 525 w, 465 w.

Bis(octaethyporphyrinato)uranium(IV), $U(OEP)_2$

To H_2OEP (0.75 g, 1.4 mmol) slurried in toluene (120 mL) was added $U(NEt_2)_4$ (0.8 mmol) dissolved in pentane (6 mL). The solution was stirred for 7 days at 20°C, and then heated for 12 h at 90°C. After being cooled to 20°C, the solution was taken to dryness. The residue was extracted with pentane (200 mL), and the solution was filtered and concentrated to *ca.* 50 mL. The brown-black pentane extract was applied to a 10 × 5 cm column of silica gel (wet packed with pentane) and the column was washed exhaustively with pentane (*ca.* 500 mL) to remove grease. The black silica gel at the top of the column was removed and extracted with chloroform (*ca.* 50 mL). The chloroform extract was filtered through an ultra fine sintered glass disc and taken to dryness to give pure $U(OEP)_2$. Material thus

purified is usually free of H_2OEP; this may be confirmed by UV-Visible spectroscopy in $CHCl_3$ by addition of a few crystals of p-toluenesulfonic acid (PTSA): the absence of an absorption at 409 nm (H_4OEP^{2+} Soret) indicates that the material is pure. Free H_2OEP can be removed from the product by treatment with PTSA in $CHCl_3$ followed by chromatography on silica gel with $CHCl_3$ as the eluent. $U(OEP)_2$ elutes quickly with the solvent front. Yield: 0.4 g (44%). UV-Vis (toluene, nm): 386 (Soret), 539, 583, 663, 730 sh. FD MS: parent on envelope m/z 1297. ^1H NMR ($CDCl_3$, 20°C): δ −1.17 (t, J_{HH} = 6.8 Hz, CH_3), −1.55 (dq, J_{HH} = 6.5 Hz, J_{HH} = 13 Hz, CH_2), −3.43 (dq, J_{HH} = 6.5 Hz, J_{HH} = 13 Hz, CH_2), −5.25 (s, fwhm = 6.5 Hz, meso-H).

Bis(octaethylporphyrinato)thorium(IV), $Th(OEP)_2$

To H_2OEP (0.50 g, 0.94 mmol) slurried in toluene (80 mL) was added $Th(NEt_2)_4$ (0.51 mmol) dissolved in pentane (6 mL). The mixture was stirred for 7 days at 20°C and then was heated for 12 h at 90°C. After being cooled to 20°C, the solution was taken to dryness. The reaction mixture was subsequently treated as described for the uranium complex (see above). Yield: 0.35 g (57%). UV-Vis (toluene, nm): 381 (Soret), 533, 576, 635, 710 sh. FD MS: parent ion envelope m/z 1303. ^1H NMR ($CDCl_3$, 20°C): δ 9.18 (s, fwhm = 5.4 Hz, meso-H), 4.11 (dq, J_{HH} = 7.5 Hs, J_{HH} = 15 Hz, CH_2), 3.89 (dq, J_{HH} = 7.5 Hz, J_{HH} = 15 Hz, CH_2), 1.70 (t, J_{HH} = 7.6 Hz, CH_3).

(Octaethylporphyrinato)(tetraphenylporphyrinato)thorium(IV), Th(OEP)(TPP)

H_2OEP (0.40 g, 0.75 mmol) and H_2TPP (0.46 g, 0.75 mmol) were slurried in toluene (100 mL) and a solution of $Th(NMe_2)_4$ (0.30 g, 0.58 mmol) in pentane (10 mL) was added. The mixture was refluxed for 36 h, and the reaction was complete as judged by UV-Vis spectroscopy. The toluene was removed by rotary evaporation. Purification was achieved using column chromatography on silica gel. The unreacted H_2OEP and H_2TPP can be eluted using a 1:3 toluene: hexane mixture. Using a 1:1 toluene:hexane mixture, the desired Th(OEP)(TPP) elutes as a brown band. (Subsequent use of neat dichloromethane elutes the $Th(TPP)_2$ formed during the reaction). The desired fraction was filtered through a fine frit and taken to dryness to give Th(OEP)(TPP). Yield 0.40 g (50%). *Anal.* Calcd. for $C_{80}H_{72}N_8Th$: C, 69.8; H, 5.27; N, 8.13; Th, 16.9. Found: C, 69.5; H, 5.15; N, 7.94; Th, 17.6. UV-Vis (toluene, nm, log ε): 393 (5.56), 486 (4.11), 544 (4.17), 584 (3.81), 638 (3.63). FD MS: parent ion envelope m/z 1376.2. ^1H NMR (CD_2Cl_2, 20 °C): δ 9.47 (br, TPP o-H), 9.22 (s, OEP meso-H), 8.24 (s, TPP pyrrole-H), 8.22 (br, TPP m-H), 7.77 (t, J_{HH} = 7.6 Hz, TPP p-H), 7.31 (br, TPP m-H), 6.67 (br, TPP o-H), 4.14, 3.86 (dq, J_{HH} = 7.4, 15 Hz, OEP CH_2), 1.46 (t, J_{HH} = 8 Hz, OEP CH_3). IR (cm^{-1}): 1596 w, 1518 w, 1321 m, 1267 m, 1195 w, 1178 w, 1142 m, 1107 w, 1057 m, 1013 m 983 s, 955 s, 909 w, 840 m, 796 s, 752 s, 702 m, 658 w, 578 w.

Bis(tetraphenylporphyrinato)uranium(IV) Hexachloroantimonate, $[U(TPP)_2^+][SbCl_6^-]$

To a mixture of $U(TPP)_2$ (391 mg, 0.27 mmol) and phenoxathiinylium hexachloroantimonate (148 mg, 0.28 mmol) was added CH_2Cl_2 (50 mL). The reaction

mixture immediately became brown, and stirring was continued for 1 h. The mixture was filtered, concentrated to 20 mL, diluted with toluene (50 mL), and allowed to stand without agitation for 12 h. The resultant purple-blue precipitate was isolated by filtration and dried in vacuum. Yield: 0.38 g (65%). *Anal.* Calcd. for $[U(TPP)_2^+][SbCl_6^-]\cdot 2C_7H_8\cdot 2CH_2Cl_2$, $C_{104}H_{78}USbCl_{10}$: C, 58.0; H, 3.7; N, 5.2; U, 11.1; Sb, 5.7; Cl, 16.5. Found: C, 58.7; H, 3.6; N, 4.9; U, 10.9; Sb, 5.7; Cl, 17.1. UV-Vis-NIR (CH_2Cl_2, nm): 392 ($\varepsilon \approx 10^5$, Soret), 1270 ($\varepsilon \approx 10^3$, fwhm = 140 nm). ^1H NMR (CD_2Cl_2, −60°C): δ 9.00 (d, J_{HH} = 6.2 Hz, o-H), 8.85 (s, fwhm = 18 Hz, m-H), 5.80 (t, J_{HH} = 7.0 Hz, p-H), 3.82 (s, fwhm = 27 Hz, m-H), 0.47 (s, fwhm = 30 Hz, m-H), -3.48 (s, fwhm = 29 Hz, pyrrole-H). X-band EPR (solid state, 7K): $g_{\parallel} = 3.1749$, $g_{\perp} = 1.3425$. IR (cm^{-1}): 3137 w, 3115 w, 3053 w, 2679 w, 2603 w, 2548 w, 2359 w, 2339 w, 2155 w, 1970 w, 1908 w, 1825 w, 1596 w, 1574 w, 1524 w, 1441 sh, 1413 m, 1333 m, 1307 m, 1275 m, 1265 m, 1218 w, 1175 s, 1076 m, 1030 w, 1003 m, 977 s, 969 sh, 896 w, 880 w, 858 w, 831 sh, 822 m, 804 m, 796 sh, 758 s, 730 s, 723 s, 705 s, 669 w, 658 w, 635 w, 621 w, 579 w, 569 w, 524 w, 497 w, 466 w.

Bis(tetraphenylporphyrinato)thorium(IV) Hexachloroantimonate, $[Th(TPP)_2^+][SbCl_6^-]$

To a mixture of $Th(TPP)_2$ (0.47 g, 0.32 mmol) and phenoxathiinylium hexachloroantimonate (174 mg, 0.33 mmol) was added CH_2Cl_2 (50 mL). The reaction mixture immediately became brown, and stirring was continued for 1 h. The solution was filtered, concentrated to 20 mL, diluted with toluene (50 mL), and allowed to stand without agitation for 12 h. The solution was filtered to give a purple blue powder. The powder was redissolved in CH_2Cl_2 (20 mL), and the solution was diluted with pentane (50 mL), and allowed to stand for 12 h. The powder was collected by filtration and dried in vacuum. Yield: 225 mg (40%). *Anal.* Calcd. for $[Th(TPP)_2^+][SbCl_6^-]$, $C_{88}H_{56}N_8ThSbCl_6$: C, 59.0; H, 3.2; N, 6.3; Th, 13.0; Sb, 6.8; Cl, 11.9. Found: C, 58.3; H, 3.3; N, 5.8; U, 12.9; Sb, 6.6; Cl, 12.9. UV-Vis-NIR (CH_2Cl_2, nm): 396 ($\varepsilon \approx 10^5$, Soret), 1480 ($\varepsilon \approx 10^3$, fwhm = 300 nm). X-band EPR (solid state, 77 K): g = 2.0016 (peak-to-peak linewidth = 6.4 G). IR (cm^{-1}): 3135 w, 3110 w, 3055 w, 2594 w, 2555 w, 2466 w, 2352 w, 2379 w, 2177 w, 1985 w, 1967 w, 1826 nm, 1709 w, 1595 m, 1574 m, 1521 w, 1493 sh, 1478 sh, 1441 m, 1412 w, 1386 s, 1333 m, 1317 w, 1297 s, 1265 s, 1220 m, 1192 sh, 1182 sh, 1161 s, 1085 sh, 1075 s, 1028 m, 1003 s, 980 s, 934 w, 896 w, 880 m, 857 m, 820 s, 804 m, 795 w, 758 s, 731 s, 723 sh, 705 s, 670 w, 657 m, 635 w, 621 w, 569 w, 534 w, 521 w, 495 w, 467 w.

(Octaethylporphyrinato)(tetraphenylporphyrinato)thorium(IV) Hexachloroantimonate, $[Th(OEP)(TPP)^+][SbCl_6^-]$

To a mixture of Th(OEP)(TPP) (0.25 g, 0.18 mmol) and phenoxathiinylium hexachloroantimonate (0.107 g, 0.20 mmol) was added CH_2Cl_2 (50 mL) and the mixture was stirred for 12 h at room temperature. The solution was filtered, concentrated to *ca.* 20 mL, and layered with toluene (70 mL). After the solvents had diffused overnight, the purple microcrystals were collected by filtration and dried under vacuum. Yield 0.186 g (60%). *Anal.* Calcd. for $[Th(OEP)(TPP)^+][SbCl_6^-]\cdot CH_2Cl_2$, $C_{81}H_{74}N_8ThSbCl_8$: C, 54.1; H, 4.15; N, 6.24; Th, 12.9; Sb, 6.78;

Cl, 15.8. Found: C, 54.7; H, 4.62; N, 6.21; Th, 13.0; Sb, 6.72; Cl, 16.1. UV-Vis (CH_2Cl_2, nm): 370 ($\varepsilon \approx 10^5$, Soret), 552, 1318 ($\varepsilon \approx 10^3$, fwhm = 220 nm). X-band EPR (1:1 C_7H_8:CH_2Cl_2): 100 K: g = 2.010 (peak-to-peak linewidth = 5.11 G) 293 K: g = 2.011 (peak-to-peak linewidth = 3.16 G). IR (cm^{-1}): 2599 w, 2449 w, 2346 w, 2183 w, 1595 w, 1524 s, 1431 s, 1318 s, 1258 w, 1227 m, 1193 w, 1181 w, 1140 m, 1129 m, 1092 w, 1059 s, 1012 s, 1004 m, 979 s, 954 s, 908 w, 880 w, 852 m, 802 m, 760 m, 731 m, 706 m, 696 m, 666 w.

Bis(tetraphenylporphyrinato)uranium(IV) Bis(hexachloroantimonate), $[U(TPP)_2^{2+}][SbCl_6^-]_2$

To a mixture of $U(TPP)_2$ (313 mg, 0.214 mmol) and phenoxathiinylium hexachloroantimonate (249 mg, 0.466 mmol) was added CH_2Cl_2 (50 mL). The reaction mixture quickly became green, and stirring was continued for 1 h. The precipitate that formed was collected by filtration and was washed with CH_2Cl_2 (3 × 50 mL) until the washings were colorless. The blue-purple solid was dried under vacuum. Yield: 322 mg (65%). *Anal.* Calcd. for $[U(TPP)_2^{2+}][SbCl_6^-]_2 \cdot 2CH_2Cl_2$, $C_{90}H_{60}N_8USb_2Cl_{16}$: C, 47.0; H, 2.6; N, 4.9; U, 10.3; Sb, 10.6; Cl, 24.6. Found: C, 46.5; H, 2.5; N, 4.7; U, 10.2; Sb, 10.9; Cl, 24.0. UV-Vis-NIR (CH_3CN, nm): 396 ($\varepsilon \approx 10^5$, Soret), 990 ($\varepsilon \approx 10^3$, fwhm = 200 nm), 1270 nm. ^1H NMR (CD_3CN, 20 °C): δ 8.40 (s, fwhm = 19 Hz, o-H), 7.56 (s, fwhm = 18 Hz, m-H), 5.95 (s, fwhm = 14 Hz, p-H, 4.88 (s, fwhm = 32 Hz, m-H), 4.15 (s, fwhm = 93 Hz, pyrrole-H)), −1.73 (s, fwhm = 23 Hz, o-H). IR (cm^{-1}): 3145 w, 3123 w, 3053 w, 2169 w, 1985 w, 1967 w, 1914 w, 1840 m, 1826 w, 1595 w, 1575 m, 1540 m, 1481 s, 1442 s, 1405 m, 1380 s, 1348 s, 1322 m, 1270 s, 1219 s, 1158 s, 1086 s, 1030 w, 1002 s, 975 s, 960 s, 923 w, 892 w, 879 m, 861 w, 852 w, 817 s, 805 m, 764 sh, 756 s, 731 s, 720 m, 705 s, 669 m, 658 m, 636 m, 619 m, 594 w, 581 w, 567 m, 519 m, 491 w, 443 w, 426 m, 408 w.

Bis(tetraphenylporphyrinato)thorium(IV) Bis(hexachloroantimonate), $[Th(TPP)_2^{2+}][SbCl_6^-]_2$

To a mixture of $Th(TPP)_2$ (288 mg, 0.198 mmol) and phenoxathiinylium hexachloroantimonate (246 mg 0.460 mmol) was added CH_2Cl_2 (50 mL). The reaction mixture quickly became green, and stirring was continued for 1 h. The precipitate that formed was collected by filtration and was washed with CH_2Cl_2(3 × 50 mL) until the washings were colorless. The blue-purple solid was dried under vacuum. Yield: 315 mg (69%) *Anal.* Calcd. for $[Th(TPP)_2^{2-}][SbCl_6^-]_2 \cdot 2CH_2Cl_2$, $C_{90}H_{60}N_8ThSb_2Cl_{16}$: C, 47.1; H, 2.6; N, 4.9; Th, 10.1; Sb, 10.6; Cl, 24.7. Found: C, 46.2; H, 2.7; N, 4.5; Th, 9.9; Sb, 11.6; Cl, 24.4. UV-Vis-NIR (CH_3CN, nm): 399 ($\varepsilon \approx 10^5$, Soret), 1080 ($\varepsilon \approx 10^3$, fwhm = 290 nm), 1487. ^1H NMR (CD_3CN, 20°C): δ 7.55 (s, fwhm = 33 Hz, o-H), 7.47 (s, fwhm = 35 Hz, m-H), 7.37 (s, fwhm = 20 Hz, p-H), 6.98 (s, fwhm = 40 Hz, m-H), 6.30 (s, fwhm = 42 Hz, o-H). IR (cm^{-1}): 3144 w, 3121 w, 3054 w, 2361 w, 2341 w, 2168 w, 1998 w, 1986 w, 1967 w, 1915 w, 1840 m, 1825 w, 1727 w, 1594 w, 1575 m, 1554 w, 1536 s, 1487 sh, 1476 sh, 1442 s, 1399 s, 1347 s, 1322 m, 1284 sh, 1268 s, 1221 s, 1162 s, 1085 s, 1030 w, 1002 s, 978 s, 961 s, 942 sh, 922 w, 880 m, 862 m, 829 sh, 817 s, 804 sh, 765 m, 757 s, 732 s, 721 m, 705 s, 669 w, 658 m, 635 m, 619 w, 593 w, 565 m, 515 m, 489 w, 442 w, 424 m, 407 w.

(Octaethylporphyrinato)(tetraphenylporphyrinato)thorium(IV) Bis(hexachloroantimonate), [Th(OEP)(TPP)$^{2+}$][$SbCl_6^-$]$_2$

To a mixture of Th(OEP)(TPP) (0.12 g, 0.087 mmol) and phenoxathiinylium hexachloroantimonate (0.117 g, 0.218 mmol) was added CH_2Cl_2 (100 mL) and the mixture was stirred for 30 hours. The solution was filtered, concentrated to *ca.* 40 mL, and layered with toluene (100 mL). After the solvents had diffused overnight, the purple-black microcrystals were collected by filtration and dried under vacuum. Yield 0.135 g (76%). *Anal.* Calcd. for $C_{80}H_{72}N_8ThSb_2Cl_{12} \cdot 1.5CH_2Cl_2$: C, 45.0; H, 3.48; N, 5.15; Th, 10.7; Sb, 11.2; Cl, 24.5. Found: C, 45.0; H, 3.97; N, 4.73; Th, 9.88; Sb, 10.2; Cl, 22.3. UV-Vis-NIR (CH_2Cl_2, nm): 364 ($\varepsilon \approx 10^5$), 582, 956 ($\varepsilon \approx 10^3$, fwhm = 160 nm). ^{1}H NMR (CD_2Cl_2, 20°C): δ 7.53 (s, TPP o-H), 7.39 (t, J_{HH} = 6 Hz, TPP p-H), 6.20 (s, TPP m-H), 5.55 (s, TPP m-H), 5.33 (s, OEP meso-H), 5.15 (s, TPP pyrrole-H), 4.97 (s, TPP o-H), 2.10, 1.82 (dq, J_{HH} = 7.5, 15 Hz, OEP CH_2), 1.02 (t, J_{HH} = 7.5, OEP CH_3). IR (cm^{-1}): 1533 s, 1422 w, 1328 w, 1262 m, 1226 s, 1180 m, 1128 m, 1086 s, 1062 s, 1018 s, 1002 s, 978 s, 955 s, 906 w, 861 m, 812 m, 764 m, 733 s, 705 s, 695 m, 656 w, 564 w, 464 m.

Crystallographic Studies

Single crystals of $Th(TPP)_2 \cdot C_7H_8$, grown by layering a chloroform solution with toluene, were mounted quickly with epoxy on thin glass fibers. [Single crystals of $Th(OEP)_2$, grown by slow evaporation of a hexane solution, were mounted on a thin glass fiber using epoxy. Subsequent comments in brackets will refer to this compound.] Standard peak search and indexing procedures yielded preliminary cell dimensions, and the crystal symmetry was verified by inspection of the axial photographs. Least squares refinement using 25 reflections yielded the cell dimensions given in Table 2.

The structure was solved by Patterson and weighted and unweighted difference Fourier methods. The position of the thorium atom was automatically deduced from a sharpened Patterson map, and partial structure expansion revealed positions for all non-hydrogen atoms in the porphyrin ring. [For $Th(OEP)_2$, the position of the thorium atom was deduced from a vector map.] Subsequent difference Fourier calculations revealed the positions of the disordered toluene molecule, which was refined as an "idealized" rigid group without hydrogen atoms. [For $Th(OEP)_2$, subsequent least-squares refinement and difference Fourier syntheses revealed positions for the remaining non-hydrogen atoms].

The quantity minimized by the least-squares program was $\Sigma w(|F_o| - |F_c|)^2$, where $w = 0.31/(\sigma(F_o)^2 + (pF_o)^2)$. [For $Th(OEP)_2$, $w = 1.26/(\sigma(F_o)^2 + (pF_o)^2)$]. The analytical approximations to the scattering factors were used, and all structure factors were corrected for both the real and imaginary components of anomalous dispersion. In the final cycle of least squares, group isotropic thermal parameters were refined for the disordered toluene carbon atom positions and for the porphyrin hydrogen atoms; the latter were included as fixed contributors in "idealized" positions with C-H = 0.95 Å. Independent isotropic thermal parameters were refined for the phenyl ring carbon atoms, and anisotropic thermal

coefficients were refined for the remaining non-hydrogen atoms. [For $Th(OEP)_2$, in the final cycle of least squares, anisotropic thermal coefficients were refined for all non-hydrogen atoms and common isotropic thermal parameters were varied for aliphatic and aromatic hydrogen atoms.] Successful convergence was indicated by the maximum shift/error of 0.106 [0.014] in the last cycle. Final refinement parameters are given in Table 2. The largest peaks in the final difference Fourier map (<1.14 e/Å^3) were located in the vicinity of the thorium atom and the disordered toluene molecule. [For $Th(OEP)_2$, the largest peaks in the final difference Fourier map were located in the vicinity of the thorium atom]. A final analysis of variance showed a slight dependence on structure factor amplitude and an inverse dependence on sin θ. [For $Th(OEP)_2$, a final analysis of variance between observed and calculated structure factors showed no systematic errors].

Single crystals of $[Th(TPP)_2^+][SbCl_6^-]\cdot 2C_7H_8\cdot CH_2Cl_2$, grown by layering a dichloromethane solution with toluene, were sealed in thin-walled glass capillaries under argon. Standard peak search and indexing procedures yielded preliminary cell dimensions, and the crystal symmetry was verified by inspection of the axial photographs. Least squares refinement using 25 reflections yielded the cell dimension given in Table 2.

The structure was solved by Patterson and weighted and unweighted difference Fourier methods. The positions of the thorium and antimony atoms were automatically deduced from a vector map, and difference Fourier calculations revealed the positions of the remaining non-hydrogen atoms of the cation and anion. Subsequent least squares difference Fourier calculations located two independent toluene solvate molecules that were disordered about a 422 symmetry point. The toluene molecules were refined as "idealized" rigid groups without hydrogen atoms. In addition to the disordered toluene molecules, there were two groups of two atomic positions that were situated nearby. These positions were assigned as partially occupied chlorine atoms of a dichloromethane solvent molecule, and these positions were independently refined to convergence. The carbon atom of the disordered dichloromethane solvate was not located, but presumably is disordered above and below the plane of the disordered chlorine atoms. The presence of dichloromethane molecules in the crystals was confirmed by microanalytical and spectroscopic data. The quantity minimized by the least-squares program was $\Sigma w(|F_o| - |F_c|)^2$, where $w = 2.54/(\sigma(F_o)^2 + (pF_o)^2)$. The analytical approximations to the scattering factors were used, and all structure factors were corrected for both the real and imaginary components of anomalous dispersion. In the final cycle of least squares, three group isotropic thermal parameters were varied: one for the hydrogen atoms, one for the disordered toluene carbon atoms, and one for the disordered chlorine atoms of the dichloromethane solvate molecules. Independent isotropic coefficients were varied for atoms C(6) and C(10), and anisotropic thermal coefficients were refined for the remaining non-hydrogen atoms. Successful convergence was indicated by the maximum shift/error of 0.040 in the last cycle. Final refinement parameters are given in Table 2. The largest peaks in the final difference Fourier map were located in the vicinity of the disordered toluene molecules. A final analysis of variance between observed and calculated structure factors showed a slight dependence on structure factor amplitude and an inverse dependence on sin θ.

Acknowledgements

We appreciate the support of the National Institutes of Health (HL-25934), the Department of Energy (DEFG02-91ER45439) for partial student support, and the Petroleum Research Fund administered by the American Chemical Society.

Supplemental Materials

Observed and calculated structure factors for the X-ray diffraction crystal structures discussed in this manuscript are available from the authors upon request.

References

1. J.W. Buchler, J. Hüttermann, J. Löffler, *Bull. Chem. Soc. Jpn.* **61**, 71 (1988).
2. (a) J.W. Buchler, H.-G. Kapellmann, M. Knoff, K.-L. Lay, S. Pfeifer, *Z. Naturforsch* **38b**, 1339 (1983). (b) J.W. Buchler, J. Fischer, M. Kihn-Botulinski, H. Paulus, R. Weiss, *J. Am. Chem. Soc.* **108**, 3652 (1986). (c) J.W. Buchler, K. Elslässer, M. Kihn-Botulinski, B. Scharbert, *Angew. Chem. Int. Ed. Engl.* **25**, 286 (1986). (d) J.W. Buchler, B. Scharbert, *J. Am. Chem. Soc.* **110**, 4272 (1988). (e) J. W. Buchler, A. De Cian, J. Fischer, P. Hammerschmitt, J. Loffler, B. Scharbert, R. Weiss, *Chem. Ber.* **122**, 2219 (1989). (f) J.W. Buchler, P. Hammerschmitt, I.Kaufeld, J.Löffler, *Chem. Ber.* **124**, 2151 (1991).
3. (a) G.S. Girolami, S.N. Milam, K.S. Suslick, *Inorg. Chem.* **26**, 343 (1987). (b) G.S. Girolami, S.N. Milam, K.S. Suslick, *J. Am. Chem. Soc.* **110**, 2011 (1988).
4. (a) K. Kim, W.S. Lee, H.-J. Kim, S.-H. Cho, G.S. Girolami, P.A. Gorlin, K.S. Suslick, *Inorg. Chem.* **30**, 2652 (1991). (b) H.-J. Kim, D. Whang, J. Kim, K. Kim, *Inorg. Chem.* **31**, 3882 (1992). (c) J.W. Buchler, A. De Cian, J. Fischer, P. Hammerschmitt, R. Weiss, *Chem. Ber.* **124**, 1051 (1991). (d) J.W. Buchler, A. De Cian, S. Elschner, J. Fischer, P. Hammerschmitt, R. Weiss, *Chem. Ber.* **125**, 107 (1992).
5. (a) J. Diesenhofer, O. Epp, K. Miki, R. Huber, H. Michel, *J. Mol. Biol.* **180**, 385 (1984). (b) T. O. Yeates, H. Komiya, A. Chirino, D.C. Rees, J.P. Allen, G. Feher, *Proc. Natl. Acad. Sci. U.S.A.* **85**, 7993 (1980). (c) O. El-Kabbani, C.-H. Chang, D. Tiede, J. Norris, M. Schiffer, *Biochemistry* **30**, 5361 (1991).
6. (a) M.S. Davis, A. Forman, L.K. Hanson, J.P. Thornber, J. Fajer, *J. Phys. Chem.* **83**, 3325 (1979). (b) W.W. Parson, A. Warshel. *J. Am. Chem. Soc.* **109**, 6152 (1987). (c) S.G. Boxer, R. A. Goldstein, D. J. Lockhart, T. R. Middendorf, L. Takiff, *J. Phys. Chem.* **93**, 8280 (1989).
7. G.S. Girolami, P.A. Gorlin, K.S. Suslick, *Inorg. Chem.* **33**, 626 (1994).
8. (a) R.J. Donohoe, J.K. Duchowski, D.F. Bocian, *J. Am. Chem. Soc.* **110**, 6119 (1988). (b) J.K. Duchowski, D.F. Bocian, *Inorg. Chem.* **29**, 4158 (1990). (c) J.K. Duchowski, D.F. Bocian, *J. Am. Chem. Soc.* **112**, 3312 (1990). (d) J.-H. Perng, J.K. Duchowski, D.F. Bocian, *J. Phys. Chem.* **94**, 6684 (1990). (e) J. -H. Perng, J. K. Duchowski, D. F. Bocian, *J. Phys. Chem.* **95**, 1319 (1991). (f) P.C. Martin, J. Arnold, D.F. Bocian, *J. Phys. Chem.* **97**, 1332 (1993).
9. (a) X. Yan, D. Holten, *J. Phys. Chem.* **92**, 409 (1988). (b) O. Bilsel, J. Rodriguez, D. Holten, *J. Phys. Chem.* **94**, 3508 (1990). (c) O. Bilsel, J. Rodriguez, D. Holten, G.S. Girolami, S.N. Milam, K.S. Suslick, *J. Am. Chem. Soc.* **112**, 4075 (1990). (d) O. Bilsel, J.W. Buchler, P. Hammerschmitt, J. Rodriguez, D. Holten. *Chem. Phys. Lett.* **182**, 415 (1991). (e) O. Bilsel, J. Rodriguez, S.N. Milam, P.A. Gorlin, G.S. Girolami, K.S. Suslick, D. Holten. *J. Am. Chem. Soc.* **114**, 6528 (1992). (f) O. Bilsel, S.N. Milam, G.S. Girolami, K.S. Suslick, D. Holten, *J. Phys. Chem.* **97**, 7216 (1993).
10. M. Gouterman, *The Porphyrins*, D. Dolphin (Ed) (Academic Press: New York, 1979; Vol. III) pp. 1–78.
11. A. Dormond, B. Belkalem, P. Charpin, M. Lance, D. Vigner, G. Folcher, R. Guilard. *Inorg. Chem.* **25**, 4785 (1986).
12. A similar shielding effect has been observed in Ce(OEP)(TPP) (Reference 2e).
13. R.H. Felton, *The Porphyrins*, D. Dolphin (Ed) (Academic Press: New York, 1979; Vol V) pp. 53–125.

14. E.T. Shimomura, M.A. Phillippi, H.M. Goff, W.F. Scholz, C.A. Reed, *J.Am. Chem. Soc.*, **103**, 6778 (1981).
15. Y. Le Mest, M. L'Her, N.H. Hendricks, K. Kim, J.P. Collman, *Inorg. Chem.* **31**, 835 (1992).
16. (a) A. Osuka, K. Maruyama, *J. Am. Chem. Soc.*, **110**, 4454 (1988). (b) C.A. Hunter, J.K.M. Sanders, A. Stone, *J. Chem. Phys.* **113**, 395 (1989). (c) T.H. Tran-Thi, J.F. Lipskier, P., Maillard, M. Momenteau, J-M. Lopez-Castillo, J.-P. Jay-Gerin, *J. Phys. Chem. 96*, 1073 (1992).
17. J.A. Hermann, J.A. Suttle, *Inorg. Synth.* **5**, 143 (1978).
18. A.D. Adler, F.R. Longo, J.D. Finarelli, *J. Org. Chem.* **32**, 476 (1967).
19. (a) C.B. Wang, C.K. Chang, *Synthesis*, 548 (1979). (b) J.B. Paine, D. Dolphin, *J. Org. Chem.* **50**, 5598 (1985). (c) V. Cerchez, *Bull. Soc. Chem. Fr.* **47**, 1279 (1930).
20. P. Gans, J-C. Marchon, C.A. Reed, J.R. Regnard, *Nouv. J. Chem.* **5**, 203 (1981).
21. (a) R.G. Jones, G. Karmas, G.A. Martin, H.J. Gilman, *J. Am. Chem. Soc.*, **78**, 4285 (1956). (b) J.G. Reynolds, A. Zalkin, D.H. Templeton, N.M. Edlestein, L.K. Templeton. *Inorg. Chem.* **15**, 2498 (1976).
22. G.W. Watt, K.F. Gadd, *Inorg. Nucl. Chem. Lett.* **9**, 203 (1973).